Water: How does it influence the $CaCO_3$ formation?

Huachuan Du and Esther Amstad*

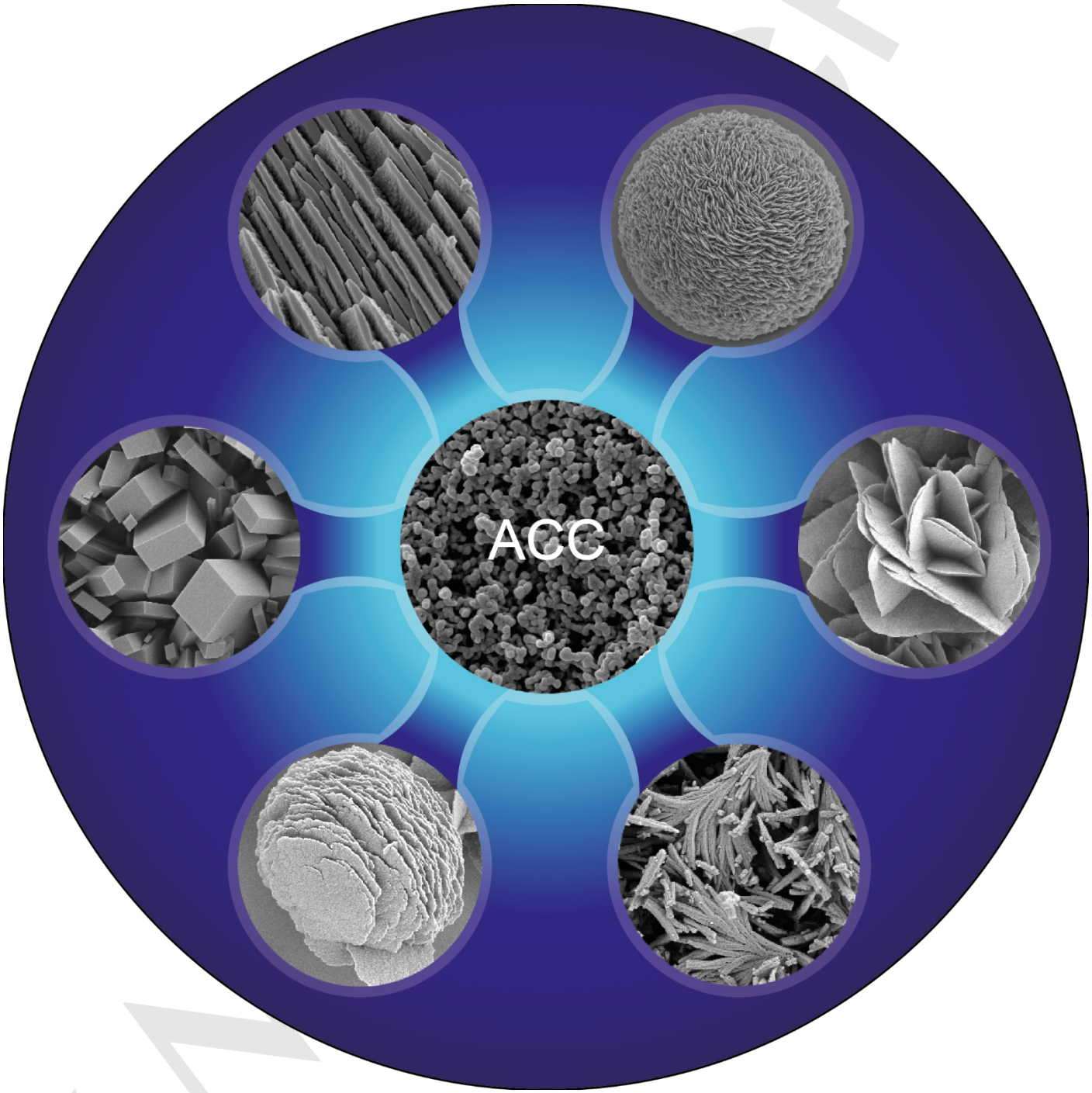

Abstract: Nature produces biomineral-based materials with a fascinating set of properties using only a limited number of elements. This set of properties is obtained by closely controlling the structure and local composition of the biominerals. We are far from obtaining a same degree of control over the properties of synthetic biomineral-based composites. A contributing reason for this inferior control is our incomplete understanding of the influence of the synthesis conditions and additives on the structure and composition of the forming biominerals. In this review, we provide an overview over the current understanding of the influence of synthesis conditions and additives during different formation stages of $CaCO_3$, one of the most abundant biominerals. We relate this influence to the structure, composition, and properties of resulting $CaCO_3$ crystals and summarize currently known means to tune these correlations. Throughout the review, we put special emphasis on the role of water in mediating the formation of $CaCO_3$ and thereby influencing its structure and properties, an often overlooked aspect that is of high relevance.

1. Introduction

Nature fabricates biomineral-based materials with a fascinating combination of properties from a limited number of elements.[1] This wide range of properties that can be accessed by nature is enabled by its tight control over the structure and local composition of biominerals.[2,3] A prominent example of biominerals that nature uses to build exceptionally strong and tough materials is calcium carbonate, $CaCO_3$. Strong and tough $CaCO_3$-based materials, such as nacre, can be formed by nature because it possesses an exquisite control over the timing, orientation, size, and morphology of the forming $CaCO_3$.[4–6] Moreover, it can precisely control the structure of $CaCO_3$ even though numerous polymorphs, including an amorphous form, three anhydrous, and two hydrated crystalline forms exist. This level of control is most likely at least in parts related to the crystallization pathway of $CaCO_3$ and the ability of certain soluble additives present in natural organisms, including acidic proteins and Mg^{2+} ions, to influence it.[4–6]

Inspired by the fascinating properties of natural $CaCO_3$-based materials, a lot of work has been devoted to gaining a better understanding of the crystallization pathway of $CaCO_3$ in nature.[7–10] $CaCO_3$ typically crystallizes via amorphous $CaCO_3$ (ACC) phases that act as transient precursors. In many organisms such as the sea urchins,[7,8,10,11] crayfishs,[12,13] corals,[14] and gastropods[15] these transient precursors are stored in designated reservoirs that serve as a temporal storage of Ca^{2+} ions. They are transported to the desired location before being rapidly transformed into $CaCO_3$ crystals. This crystallization pathway allows certain organisms to rapidly fabricate or repair load-bearing structures on demand. For example, freshwater crayfish usually store protein-stabilized ACC in their gastroliths and use it to build their exoskeleton during molting.[12,13] The presence of soluble additives can significantly influence this crystallization process such that they offer control over the composition, size, morphology, and structure of the resulting $CaCO_3$ crystals.[4,5,9] Moreover, they contribute to the outstanding mechanical properties observed in many natural $CaCO_3$-based materials.[3] An illustrative, well-characterized example is nacre that is composed of layered platelets made of aragonite, one of the metastable anhydrous crystalline $CaCO_3$ polymorphs, as shown in Figure 1A. Each platelet is made of crystalline $CaCO_3$ nanograins that all possess the same orientation and are separated by organic additives, as shown in Figure 1B.[3,16] The presence of organic additives is crucial for the mechanical properties of nacre: they enable plastic deformation of aragonite platelets if subjected to mechanical loads, thereby significantly increasing their fracture toughness.[17,18]

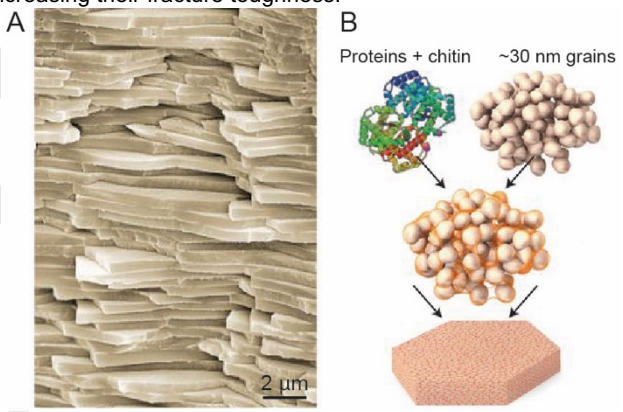

Figure 1. Structure and composition of nacre. (A) SEM image of a mollusk shell nacre composed of layered aragonite platelets. (B) Schematic illustration of the composition and structure of the platelets made of nano-crystalline aragonite grains that are separated by organic additives.[3] Figures reproduced with permission from Springer Nature.[3]

These examples hint at the importance of the formation route of $CaCO_3$ crystals via ACC precursors and the presence of soluble additives for the mechanical properties of these materials. However, how nature uses additives to control the formation of $CaCO_3$, including the formation, stabilization, and crystallization of ACC, as well as the composition, size, structure, morphology, and properties of the resulting crystals, is not fully understood.[4,5] This incomplete understanding prevents us from gaining a similar degree of control over the structure and hence properties of synthetic $CaCO_3$-based counterparts.[19]

To gain a better understanding of the $CaCO_3$ formation, $CaCO_3$ has been synthesized in the laboratory where synthesis conditions have been systematically varied in the presence and absence of additives. Particular attention has been paid to the influence of the solute concentration, pH, temperature, solvent, confinement and additives present during the $CaCO_3$ formation. All these parameters have been demonstrated to influence the

H. Du, Prof. Dr. E. Amstad
Soft Materials Laboratory
Institute of Materials
Ecole Polytechnique Fédérale de Lausanne (EPFL)
1015 Lausanne, Switzerland
E-mail: esther.amstad@epfl.ch

composition, structure, morphology, and properties of the resulting crystals. In this review, we summarize the current understanding of the influence of these parameters on the $CaCO_3$ formation. In particular, we emphasize the thermodynamic and kinetic roles of water at different stages of the $CaCO_3$ formation. The first part of this review is devoted to the different formation mechanisms of ACC that have been proposed and the characterization of the resulting amorphous precursors. Within this framework, we relate the synthesis conditions to the structure, hydration, crystallization kinetics of ACC, and the structure and morphology of the resulting crystals. The second part of this review discusses the influence of soluble additives on the formation of $CaCO_3$. A better understanding of the role of synthesis conditions and additives in the formation of $CaCO_3$ will likely offer a superior control over the structure and morphology of these materials, thereby enabling the fabrication of $CaCO_3$-based materials with properties that more closely resemble those of natural counterparts.

2. Formation of ACC

In synthetic systems, $CaCO_3$ is produced through precipitation reactions occurring between Ca^{2+} and CO_3^{2-} ions. The rate at which $CaCO_3$ forms depends on the synthesis method. A fast method to produce $CaCO_3$ is direct mixing of an aqueous solution containing Ca^{2+} ions with one containing CO_3^{2-} ions.[20–23] The reaction rate can be reduced by slowing down the diffusion of Ca^{2+} and CO_3^{2-} ions. This can be achieved, for example, by placing a membrane between two water-filled arms of a U-tube, one arm containing $CaCl_2$ and the other containing Na_2CO_3.[24–26] Similarly, the reaction rate is slowed down if CO_3^{2-} ions are formed in a Ca^{2+}-containing solution. Carbonate ions can be formed from gaseous CO_2 that is directly introduced into a $Ca(OH)_2$-containing aqueous solution to precipitate $CaCO_3$.[27–30] Similarly, carbonate ions can be continuously produced for example through the decomposition of ammonium carbonate.[31–33] Another commonly used route to slowly produce $CaCO_3$ is the Kitano method where an aqueous solution saturated with $Ca(HCO_3)_2$ is stored in an open vial. Upon storage of this solution, $Ca(HCO_3)_2$ decomposes into $CaCO_3$ by releasing CO_2.[34–37]

Different possible pathways through which $CaCO_3$ crystals form are schematically summarized in Figure 2. If the concentration of Ca^{2+} and CO_3^{2-} ions in the solutions are sufficiently low such that the solutions are supersaturated with respect to any crystalline $CaCO_3$ phase but undersaturated with respect to ACC, the formation of $CaCO_3$ crystals usually follows the classical nucleation and growth pathway.[38–40] In this case, crystalline $CaCO_3$ nuclei form and subsequently grow into larger crystals via ion-by-ion attachment process. However, in most synthetic systems, the solutions are supersaturated also with respect to ACC such that the first phase that forms is typically ACC.[22,41–44] The mechanisms of the ACC formation are still debated and most likely depend on the exact synthesis conditions.[45–48] Different types of intermediate species, such as prenucleation clusters (PNCs) and liquid precursors have been reported to precede the ACC formation, as summarized in figure 2.[35,45,49–51] Prenucleation clusters have been observed in undersaturated and supersaturated solutions using titration experiments, as exemplified in Figure 3A.[49] In addition, clusters with a well-defined diameter of around 2 nm have been observed with analytical ultracentrifugation (AUC),[49] cryogenic transmission electron microscopy (cryo-TEM),[36] and small angle X-ray scattering (SAXS).[52,53] These experimental findings are supported by molecular dynamics (MD) simulations that indicate that PNCs are dynamically ordered liquid-like oxyanion polymers (DOLLOPs) composed of alternating Ca^{2+} and CO_3^{2-} ions, as shown in Figure 3B.[54]

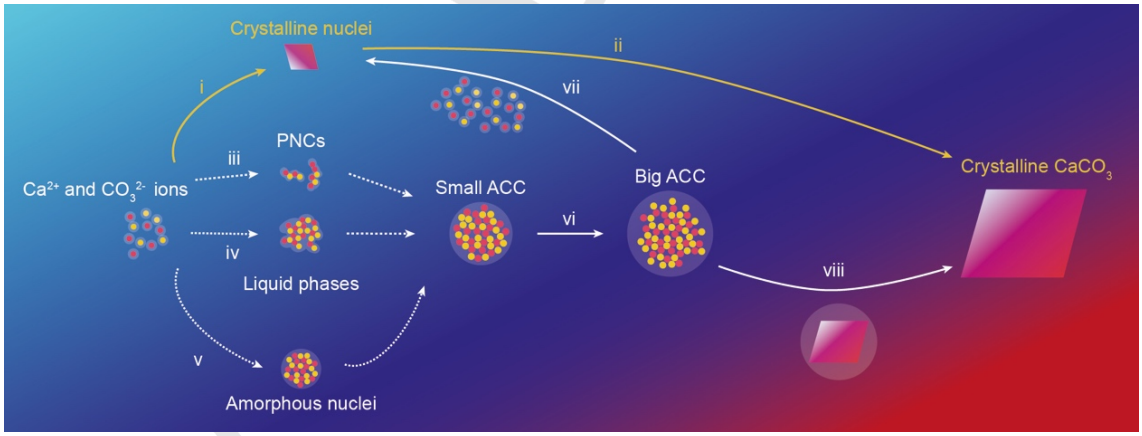

Figure 2. Schematic illustration of proposed mechanisms of the $CaCO_3$ formation. $CaCO_3$ is most often formed from aqueous solutions containing Ca^{2+} and CO_3^{2-} ions. (i,ii) Crystalline $CaCO_3$ nuclei can form and grow into big crystals through ion-by-ion attachment following the classical nucleation theory (CNT), if the solutions are supersaturated with respect to any crystalline $CaCO_3$ phase but undersaturated with respect to that of ACC. However, in most synthetic systems, the solutions are supersaturated also with respect to ACC such that the first phase that forms is typically ACC. ACC particles can form through different mechanisms: (iii) Counter ions associate with each other such that they form highly hydrated chain-like ion clusters, so-called prenucleation clusters (PNCs) that subsequently aggregate into ACC particles. (iv) An aqueous solution containing Ca^{2+} and CO_3^{2-} ions undergoes a spinodal or binodal liquid-liquid phase separation to form a solute-rich liquid phase where ACC particles form through dehydration of the liquid phase or nucleation from the liquid phase. (v) ACC nuclei directly form in the aqueous solution. (vi) The formed small ACC particles grow until they transform into crystals. This transformation can occur through a (vii) dissolution-recrystallization mechanism if ACC is in contact with bulk water or (vii) solid-state transformation if ACC is not in contact with bulk water.

Experiments and simulations suggest that the formation of PNCs, their stability and dynamic behavior is strongly influenced by water molecules that are associated with these clusters.[54,55] Based on these observations, it was suggested that ACC forms through aggregation of PNCs following a non-classical route.[45,49] However, more recent experimental studies and MD simulations do not provide evidence for the existence of significant amounts of PNCs.[46,56,57] Even if PNCs were present under certain experimental conditions, their role in the formation of ACC requires further clarification.[46] For example, these intermediate clusters have originally been proposed to be thermodynamically stable and decrease the nucleation barrier for the formation of $CaCO_3$ crystals.[49] This contrasts more recent work indicating that if PNCs are thermodynamically stable, the height of the nucleation barrier increases.[40,46]

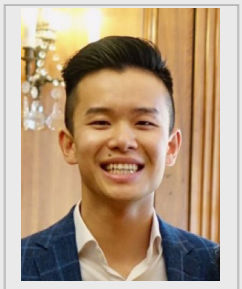

Huachuan Du obtained his B.E. degree from the Department of Polymer Materials and Engineering in the Harbin Institute of Technology (China) in 2013 and his M.S. degree from the Institue of Materials Science at Ecole Polytechnique Fédérale de Lausanne (EPFL, Switzerland) in 2015. He is currently a PhD student in the Soft Materials Laboratory at EPFL under the supervision of Prof. E. Amstad. His research focuses on understanding the early stages of the $CaCO_3$ formation and the fabrication of the bio-inspired functional materials.

Esther Amstad studied material science at ETH in Zurich, Switzerland, where she also carried out her PhD thesis under the supervision of Prof. Marcus Textor (2007-2011). As a Postdoctoral fellow, she joined the experimental soft condensed matter group of Prof. David A. Weitz at Harvard University, USA (2011-2014). Since June 2014, she is Tenure Track Assistant Professor at the Institute of Materials at EPFL, Switzerland, where she heads the Soft Materials Laboratory (SMAL). Inspired by nature, her research team develops drop-based processing routes that offer control over the local composition and structure of materials to fabricate adaptive materials with mechanical properties that are similar to those of natural counterparts.

Early stages of $CaCO_3$ crystallization are often accompanied by the formation of liquid-like precipitates, as shown in Figure 3C.[29,33,35,50] These precipitates are reported to be a result of spinodal or binodal liquid-liquid phase separations that occur over a range of temperatures and solute concentrations, as schematically shown in Figure 3D.[35,51,58] The solute-rich liquid phase, that corresponds to the liquid-like precipitates, can be stabilized with additives including Mg^{2+},[59] poly(aspartic acid) (PAsp),[33,60,61] poly(acrylic acid) (PAA),[60] and certain proteins such as ovalbumin.[62] However, how such solute-rich liquid phases transform into ACC is still unknown. A recent study suggests that the solute-rich liquid phase is composed of an assembly of polymer-stabilized ACC nanoclusters. Because of the small sizes of these clusters and their repulsive surfaces, ACC nanoclusters macroscopically display a liquid-like behavior.[63] These results suggest that the liquid-like phase is essentially a variant of ACC particles encompassing a high amount of water, well in agreement with previous reports that observed different types of ACC with different hydrations.[23,29,30,64,65] From these observations, it is questionable if the introduction of a liquid-liquid phase separation that precedes the ACC formation is required to describe the crystallization of $CaCO_3$.

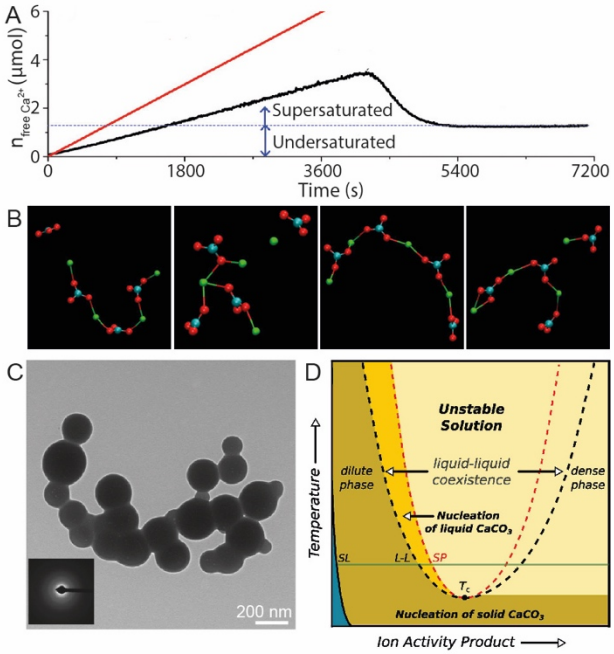

Figure 3. Formation of ACC through non-classical routes. (A) Evolution of the amount of free Ca^{2+} ions measured with a calcium ion-selective electrode when an aqueous solution containing 10 mM $CaCl_2$ is added to a carbonate buffer at pH = 9.25 at a rate of 10 μL min^{-1}, indicated in black. The total amount of Ca^{2+} ions added to the solution is indicated in red. These results suggest that a significant amount of Ca^{2+} ions is bound by CO_3^{2-} ions to form PNCs both, in solutions that are undersaturated and supersaturated with respect to ACC.[49] (B) Examples of the structures of the PNCs composed of four pairs of Ca^{2+} and CO_3^{2-} ions obtained with MD simulations. Calcium atoms are indicated in green, carbon atoms in blue, and oxygen atoms in red.[54] (C) Cryo-TEM image of liquid-like $CaCO_3$ particles that are obtained by freezing a levitated drop composed of a saturated $Ca(HCO_3)_2$ solution with liquid ethane.[35] (D) Phase diagram of aqueous solutions containing Ca^{2+} and CO_3^{2-} ions. The solubility of all crystalline $CaCO_3$ polymorphs is approximated to be the same and indicated by the solid black line SL. The liquid-liquid coexistence region is indicated by the dashed black L-L line, the spinodal decomposition region by the dashed red SP line.[51] Figures reproduced with permission from the American Association for the Advancement of Science,[49,51] Springer Nature[54] and the American Chemical Society.[35]

Several studies suggest that the ACC formation can be described using the classical nucleation and growth theory.[57,66]

The preferential formation of the ACC phase during early stages of $CaCO_3$ crystallization might be thermodynamically driven: Molecular dynamics (MD) simulations indicate that the free energy of ACC particles whose diameters do not exceed a few nanometers is below that of their crystalline counterparts.[67,68] Hence, ACC is the thermodynamically most stable phase during early stages of the $CaCO_3$ formation. A contributing reason for the lower free energy of the amorphous phase in small particles is its lower surface energy that is approximately 0.33 J/m^2.[69] If ACC particles are sufficiently small, such that their surface-to-volume ratio is high, the lower surface energy outweighs the higher bulk energy of the amorphous phase compared to any of the crystalline ones.[70] The thermodynamic stability of the ACC phase might be further increased by water that is incorporated in ACC particles and decreases their bulk free energy.[68] The preferential formation of ACC can also be kinetically driven:[4] The lower surface energy of ACC[69] results in a smaller energy barrier for nucleation, thereby accelerating the nucleation of the amorphous phase.[70] The faster formation of small amorphous particles compared to crystalline counterparts is supported by MD simulations.[68,71]

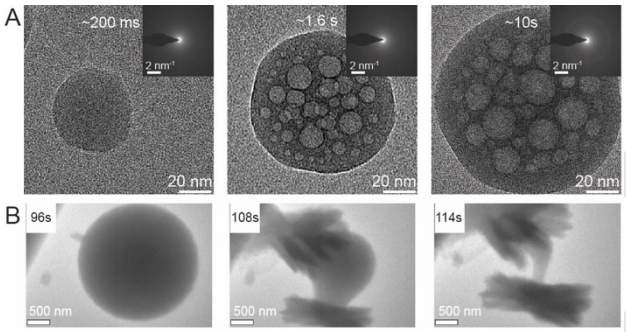

Figure 4. Growth and transformation of ACC particles in aqueous solutions. (A) TEM images of ACC particles whose formation is quenched at different stages by a microfluidic spray dryer. The electron-light phases appearing in the TEM images are caused by interactions between mobile water molecules contained in ACC and the electron beam such that the size and number of these regions provides qualitative information on the amount of mobile water contained in ACC. The corresponding SAED patterns are included as insets.[30] (B) Time-lapse TEM images of the transformation of ACC particles into crystals obtained by *in-situ* liquid cell TEM.[23] Figures reproduced with permission from the American Chemical Society,[30] and the American Association for the Advancement of Science.[23]

Small ACC nanoparticles with diameters of a few nm rapidly grow or agglomerate into bigger ones.[57,68,72,73] This growth or agglomeration reduces their surface-to-volume ratio such that, at some point, the free energy of ACC particles exceeds that of the crystalline polymorphs.[68] The higher free energy of the ACC phase is supported by calorimetric measurements that neglect the small entropy contribution. For example, the enthalpy of ACC particles with diameters above 45 nm is 3 to 15 ± 3 kJ/mol higher than that of calcite, indicating that ACC particles of these sizes are metastable.[20,74–76] Despite of their metastability, ACC particles can grow into particles with diameters reaching up to several µm within only a few seconds to minutes.[21,23,30,32,42,77] During the fast growth of ACC, significant amounts of water are incorporated into the particles,[30] as show in Figure 4A. This incorporated water decreases the enthalpy of ACC particles,[74,78,79] rendering the growth thermodynamically favorable. However, when the size of the growing ACC particles exceeds a certain value, they transform into one of the more stable crystalline forms.[23,80,81] This transformation was experimentally observed, for example, for particles whose diameter exceeds a few micrometers using *in-situ* liquid cell TEM,[23] as shown in Figure 4B.

3. Structure and hydration of ACC

The formation of ACC is influenced by synthesis conditions including the formation time,[30] solute concentration,[51,58,66,73] pH,[49,57] temperature,[51,57,58,66] solvent,[82] and confinement.[83] These conditions also influence the structure and hydration of the resulting ACC particles.[30,64,68,82,84–86] To investigate how synthesis conditions influence the structure and hydration of ACC, a thorough characterization of these parameters is key.[64,87,88] A variety of techniques that are most commonly used to characterize ACC are summarized below.

3.1. Structure

Amorphous particles do not possess any long-range order such that they do not display distinct diffraction peaks if characterized with light, electrons, and X-rays.[9,84] This feature is distinctly different from crystals and allows to experimentally easily identify the amorphous structure of particles, for example using X-ray diffraction (XRD) where diffusive and broad peaks are observed.[64,75] The amorphous structure of $CaCO_3$ particles can also be characterized on a single particle level using select area electron diffraction (SAED), as shown in Figure 4A.[30]

Complementary information on the structure of $CaCO_3$ particles and their composition can conveniently be extracted from vibrational spectroscopy measurements such as Fourier-transform infrared (FTIR) and Raman spectroscopy. The carbonate ions contained in ACC possess a different symmetry compared to those contained in crystals such that they have a different photon absorption behavior. For example, the ACC phase has a broad v_2 out-of-plane bending absorption peak at 866 cm^{-1} and no v_4 in-plane bending absorption peak in its IR spectra while calcite has a sharp v_2 peak at 874 cm^{-1} and a v_4 peak at 712 cm^{-1}, as shown in Figure 5A.[30] In addition, the ACC phase usually contains water in its structure that results in a broad absorption peak in the region of 2750–3600 cm^{-1} and a small absorption peak around 1640 cm^{-1}.[25,82] These peaks are absent in anhydrous crystalline samples. Similarly, the ACC phase displays Raman features that are distinctly different from its crystalline counterparts: The ACC phase has an intense broad peak around 1085 cm^{-1} and a broad featureless hump around 140-300 cm^{-1}, while crystalline $CaCO_3$ displays sharp peaks in these regions, as shown in Figure 5B.[89–91] In addition, crystalline $CaCO_3$ has a broad absorption peak in the range of 700–750 cm^{-1} that is absent in ACC.

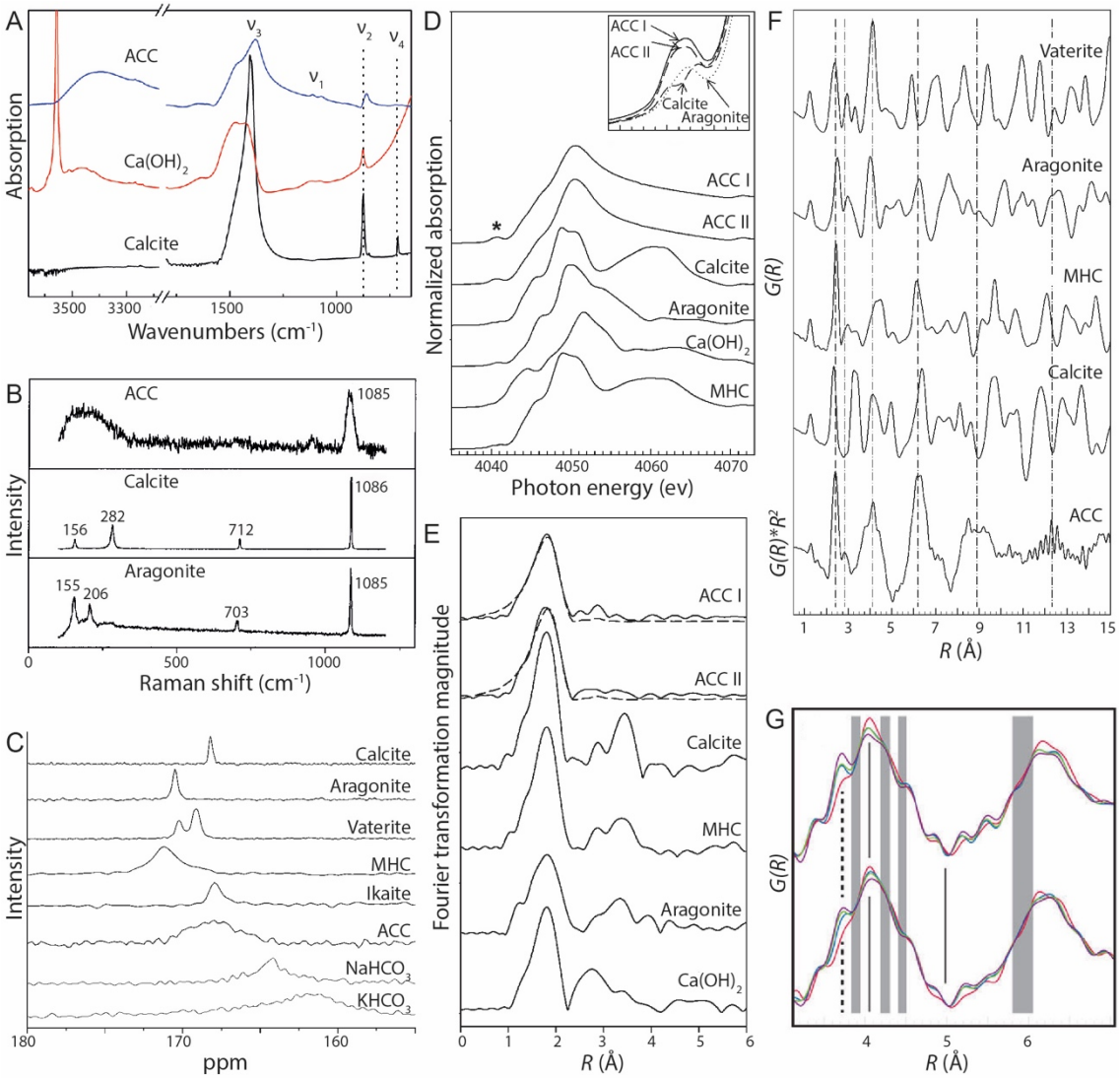

Figure 5. Characterizations of the ACC structure. (A) FTIR spectra of ACC particles, $Ca(OH)_2$ containing a small amount of calcite, and calcite.[30] (B) Raman spectra of ACC, calcite, and aragonite.[90] (C) ^{13}C MAS solid-state NMR spectra of different $CaCO_3$ phases including ACC, vaterite, aragonite, calcite, monohydrocalcite (MHC), and calcium carbonate hexahydrate (Ikaite), as well as two reference compounds, sodium hydrogencarbonate and potassium hydrogencarbonate.[92] (D) Ca K-edge XANES spectra of ACC particles that are synthesized through two different methods and four reference samples including calcite, aragonite, $Ca(OH)_2$, and MHC with (E) the corresponding measured (solid line) and fitted (dashed line) Fourier Transforms of the EXAFS undulations in R-space. The peak at ~1.8 Å measured for ACC samples after the correction for phase shift corresponds to a Ca-O distance of ~2.4 Å.[64] (F) PDF analysis of ACC and four different crystalline $CaCO_3$ phases.[64] (B) Zoom-ins of PDFs measured for ACC particles synthesized at pH=10.6 (red), pH=12.2 (blue), pH=12.5 (green), and pH=12.7 (purple).[86] Figures reproduced with permission from the American Chemical Society[30,64,86,92] and the Taylor & Francis.[90]

A powerful tool to more closely probe the chemical environment of CO_3^{2-} contained in $CaCO_3$ is ^{13}C solid-state NMR spectroscopy. Information on the structure of $CaCO_3$ can be extracted from the width of the ^{13}C peak measured with magic angle spinning (MAS) ^{13}C NMR spectroscopy. The ^{13}C peak measured for ACC is much broader than that of crystalline $CaCO_3$: The line width of the ^{13}C peak measured for ACC is around 3.6 ppm and only around 0.3 ppm for calcite, as shown in Figure 5C.[64,92] Additional information on the structure of $CaCO_3$, including its hydration,[85,92] might be extracted from the ^{13}C chemical shift measured with MAS ^{13}C NMR spectroscopy.[82,84,85,93] However, the chemical shifts measured for ACC relative to calcite vary: Some studies measure variations up to 1 ppm[84,93,94] whereas others do not observe any shifts.[64,92,95] A possible reason for these observed differences in ^{13}C chemical shifts might be varying hydrations of ACC particles that are produced under different synthesis conditions. Indeed, careful analysis of the ^{13}C chemical shift anisotropy (CSA) parameters performed using 2D $^{13}C\{^1H\}$ cross-polarization phase adjusted spinning sideband (CP PASS) NMR spectroscopy reveals that C atoms contained in CO_3^{2-} ions of hydrated ACC form hydrogen bonds with water molecules. These hydrogen bonds shift the C atoms away from the centroid of the O_3 triangular plane.[95] This positional offset of the C-atoms most likely contributes to the observed ^{13}C chemical shift of ACC.

A commonly employed technique that offers more insights into the local structure of ACC particles is X-ray absorption spectroscopy (XAS). The coordination shells of the Ca atoms can be characterized with Ca K-edge XAS measurements.[96,97] The region encompassing the main absorption peak, the X-ray Absorption Near-Edge Structure (XANES), provides qualitative information on the symmetry of the nearest neighbors of Ca atoms.[9,97,98] The different symmetries present in the structure of amorphous and crystalline $CaCO_3$ phases result in distinctly different absorption patterns. For example, Ca K-edge XANES spectra of ACC consist of a single main absorption peak around 4049 eV that does not contain any shoulder around 4045 eV. This main peak is partially convoluted with a small pre-edge peak around 4040 eV. By contrast, calcite results in two absorption peaks located around 4050 eV and 4060 eV, as shown in Figure 5D.[64] Its first main absorption peak encompasses a shoulder around 4045 eV and does not contain any pre-edge peak. More quantitative information on the ACC short-range order can be extracted from the Ca K-edge X-ray absorption fine structure (EXAFS) by fitting the undulations measured in these regions, as shown in Figure 5E.[9,64,97,98] This analysis reveals information on the average coordination number (*CN*) of O atoms around Ca atoms as well as the average distance (*R*) between O and Ca atoms. The average *CN* of ACC varies from 2 to 7 but is most frequently around 6.[64,84,85,99,100] The average *R* for ACC is typically around 2.4 Å,[64,84,85,99,100] well in agreement with values obtained from ^{43}Ca NMR[101] and MD simulations.[68,101,102]

A detailed analysis of ACC suggests that this phase has a characteristic short-range order. Whether the small differences in the short-range order are a result of the different hydrations of ACC particles produced under different synthesis conditions remains to be shown. However, it is clear that variations of the values for *CN* and *R* introduced by using different fitting procedures of EXAFS data are significant.[64,88] This uncertainty in the data analysis makes it difficult to unequivocally relate differences in the hydrations of ACC phases to their structural variations.

Information on the local structure of ACC can also be extracted from a pair distribution function (PDF) analysis that is performed on total scattering data.[64,103] This analysis indicates that ACC possesses short- and medium-range order up to a length scale of 10 Å.[64,100] In particular, PDF spectra of ACC particles reveal a prominent feature at 2.4 Å that corresponds to the first Ca-O coordination shell, in good agreement with EXAFS results,[30,64,99] as shown in Figure 5F.[64] Fits of the PDF spectra of X-ray and neutron total scattering results indicate that the number of oxygen atoms contained in the first coordination shell averages at 7, well in agreement with EXAFS results.[104] The majority of the oxygen atoms located in the first coordination shell originate from carbonate ions and the rest from water.[104] In addition, PDF data reveal two characteristic features in the medium-range length scale: One around $R = 4$ Å that can mainly be attributed to the Ca···Ca correlations and one around $R = 6$ Å that can primarily be attributed to the Ca···O correlations.[88]

These *in-depth* studies over the amorphous $CaCO_3$ structure reveal some similarities with crystalline $CaCO_3$ structures that might influence the transformation of ACC into a crystal.[84,85,87,93,99,105] These similarities have also been observed in MD simulations. These simulations reveal additional structural features of ACC that display some similarities to one of the crystalline polymorphs including the orientational-,[67,106] short-range[78] and medium-range order,[71,78] as well as the distribution of angles of the nearest-neighboring atoms.[107] However, all these similarities are subtle and in certain experimental studies they are even inexistent[64,82,86] such that they are debated. A possible reason for the variations in the reported results of the local structure of ACC particles might be related to differences in their synthesis conditions[82,84–86] and therefore their hydrations.[85] For example, if ACC particles are synthesized at increasing pHs, the intensity of the PDF peak at 3.7 Å grows on the expense of the peak at 4.1 Å, as shown in Figure 5G.[86]

3.2. Hydration

Nature frequently produces anhydrous ACC.[9] By contrast, most synthetic ACC encompasses water; this water influences the formation of ACC and its stability against crystallization.[30,68,74,75] The amount of water contained in ACC depends on the synthesis conditions: The degree of hydration (*n*) of ACC, $CaCO_3{\cdot}nH_2O$, have been reported to range from 0.4 to 1.6.[29,30,64,65,69,75,84,92,100,108] Molecular dynamics simulations and experiments reveal that the vast majority of water molecules is incorporated into the structure of ACC.[64,104] Most of this water is directly bound to Ca atoms:[101,104] 16-22% of the oxygen atoms contained in the first Ca coordination shell originate from water molecules.[102,104] Similarly, water molecules form hydrogen bonds with oxygen atoms contained in carbonate ions. Indeed, hydrogen bonds formed between water and carbonate ions are more

favorable than those between two water molecules.[79,104] These water-carbonate hydrogen bonds cause an in-plane displacement of carbon atoms contained in CO_3^{2-} away from the centroid of the O_3 triangle.[95] This distortion hampers the re-arrangement of ions, thereby stabilizing the ACC against crystallization.[95]

To obtain a better understanding of the distribution of water within ACC, a three dimensional (3D) atomic ACC model has been developed on the basis of PDF analysis. This model indicates that ACC consists of a nano-porous Ca-rich matrix encompassing a percolating network of channels that are filled with CO_3^{2-} ions and water, as shown in Figure 6A.[88] The surrounding matrix encompasses H_2O molecules that strongly interact with Ca^{2+} ions such that these molecules have a low mobility.[88,102,109] By contrast, the nanochannels contain water molecules that form weaker hydrogen bonds with CO_3^{2-} such that their mobility is much higher.[88,102,109] This result is consistent with experimental ^1H solid-state NMR measurements that reveal two types of water molecules possessing a distinctly different mobility.[64] The two different types of water molecules can also be analyzed with thermogravimetry analysis (TGA) where weakly interacting, mobile water evaporates at much lower temperatures than the strongly interacting, rigid water.[100,110,111] Due to the different binding strengths, the mobile water can be removed from ACC particles through freeze drying, in stark contrast to the rigid water.[108,112]

The existence of two types of water molecules possessing a distinctly different mobility within ACC is well accepted and has been confirmed with simulations and experiments.[30,64,79,110,111] However, the dimensions of nano-channels that are filled with mobile water are debated.[88,103,104] This uncertainty might be related to the dynamic nature of these channels: MD simulations reveal that nano-channels shrink with time due to ion re-arrangements.[78,101] These results imply that even if such channels exist during early stages of the ACC formation, they disappear on time scales that are difficult to access experimentally. Hence, experimental evidence of these nano-channels is missing.

The formation of mobile water-rich channels as big as a few nm is still debated. However, it is clear that mobile water molecules form a percolating network if the degree of hydration of ACC is sufficiently high.[79,104] Simulations suggest that percolating water networks form if the degree of hydration of ACC exceeds 0.8.[79] If the degree of hydration falls below this threshold value, the mobility of water molecules and ions significantly decreases.[79] This observation suggests that the majority of water contained in ACC with *n* below 0.8 is rigid. This suggestion is in line with TGA results that reveal an *n* below 0.8 for ACC samples that have been treated at temperatures around 100°C to remove the mobile water.[64,111]

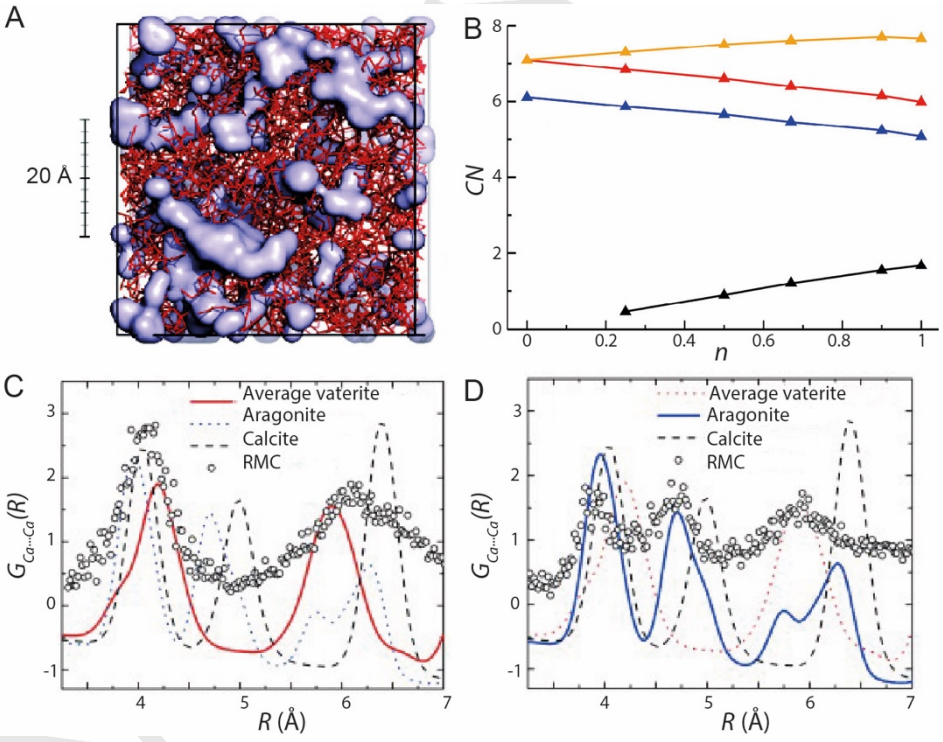

Figure 6. Hydration of ACC and its influence on the ACC short- and medium-range order. (A) Stereo representation of an atomic 3D model of the nanoporous structure of ACC. The Ca-rich frameworks are indicated by the red sticks, the water-rich nanochannels by the blue surfaces.[88] (B) Average *CN* of O (orange) and C (blue) atoms within the first coordination shell of Ca as function of the degree of hydration (*n*) of ACC as determined by MD simulations. The oxygen atoms contributed by water molecules are indicated in black, those contributed by carbonate ions in red.[78] (C, D) Average Ca···Ca correlations in (C) as-synthesized ACC particles and (D) those exposed to a pressure of 11.9 GPa obtained from reverse Monte-Carlo (RMC) modelling of their PDFs. They are compared to that of calcite, aragonite, and vaterite at ambient pressure.[105] Figures reproduced with permission from the American Chemical Society[78,88] and John Wiley & Sons.[105]

Water contained in ACC particles can influence their short- and medium-range order. A dehydration of ACC is thus accompanied by a re-arrangement of ions, as indicated by MD simulations.[78,79,102,109] During dehydration, H_2O molecules present in the first Ca-O coordination shell are replaced by CO_3^{2-} groups. As a result of this exchange, the values of *CN* and *R* in the first Ca-O coordination shell remain nearly constant, as shown in Figure 6B.[78,104] Hence, it is difficult to experimentally quantify structural differences for ACC particles possessing different degrees of hydration with commonly used methods such as EXAFS. Yet, these differences can be qualitatively assessed by comparing XANES or PDF spectra of ACC particles subjected to elevated temperatures or pressures such that their degree of dehydration changes *in situ*. Interestingly, *in-situ* XANES measurements reveal shifts of the Ca absorption edge towards lower values when *n* decreases from 1.4 to 0.7 upon exposure to elevated temperatures.[30] By contrast, no shift could be detected if *n* does not fall below 1, a value above the percolation threshold of *n*~0.8. These observations imply that measurable structural rearrangements occur only when rigid water is removed and this is the case if the degree of hydration is below the percolation threshold. These XANES results are supported by small changes in the relative EXAFS peak intensities and different PDF features, that could only be observed if *n* falls below 0.8.[74,100,104] Structural changes in ACC could also be monitored with PDF if the dehydration is induced with uniaxial pressures as high as 12 GPa. This dehydration is accompanied by a re-arrangement of ions into a structure that displays some resemblance with aragonite, as demonstrated with PDF in Figures 6C and D.[105] More generally, it has been suggested that the denser structure of partially or fully dehydrated ACC might display some resemblance with one of the anhydrous crystalline $CaCO_3$ polymorphs.[78,106,107,109]

Some synthesis conditions, including the pH,[84–86] solvent,[82] and temperature[85] of the solution that ACC is produced from influence the water-ion interactions within ACC.[69,85] Hence, these parameters also influence the ratio of mobile to rigid water present in ACC and therefore its local structure. Interestingly, many ACC particles produced under varying synthesis conditions possess a similar degree of hydration. This observation suggests that the degree of hydration is insufficient to characterize ACC. Instead, the ratio of mobile to rigid water must also be considered.

4. Crystallization of ACC

ACC particles with diameters exceeding a few nanometers are metastable and tend to transform into crystals with time. The kinetics of this crystallization and the structure and morphology of the resulting crystals can be significantly influenced by the crystallization pathway.[65,69,74,111] Different ACC crystallization mechanisms have been proposed in the last decade, as schematically summarized in Figure 2. A particularly important parameter that determines the crystallization pathway is the presence of bulk water in the crystallization environment: In the presence of bulk water, crystallization often occurs through the so-called dissolution-recrystallization mechanism. By contrast, in the absence of bulk water, ACC particles typically crystallize through solid-state transformations. In both cases, the propensity of ACC particles to crystallize primarily depends on their *kinetic* stability that is, at least in parts, influenced by the hydration of ACC, as summarized below.

4.1. Solid-state transformation

To convert ACC particles into crystals via solid-state transformation, they must be dehydrated before anhydrous crystalline nuclei form.[65,78] The dehydration process of ACC was initially proposed to be thermodynamically favored because the enthalpy of hydrated ACC particles measured with isothermal acid solution calorimetry was higher than that of anhydrous ones measured with differential scanning calorimetry (DSC).[75] This thermodynamic argument has often been used to describe the solid-state transformation of biogenic ACC under ambient conditions.[10,15,75,113,114] However, more recent experiments that assessed the enthalpy of ACC before and after its dehydration using the same technique reveal that dehydrated ACC particles possess a higher enthalpy.[74,100] These more recent experimental results are supported by MD simulations that suggest the dehydration to be thermodynamically unfavorable, as shown in Figure 7A.[68,78,79] To overcome the energy penalty associated with the dehydration, ACC must be exposed to external triggers such as elevated temperatures,[69,74,86,111] pressures,[115,116] or an electron beam.[29]

Dehydration of ACC is associated with a re-arrangement of ions contained in ACC. [30,74,78,79,100,104] This re-arrangement is kinetically hindered by the interactions between water and ions contained in ACC, that decrease the mobility of water and ions.[78,88,95] In the early stage of dehydration where the degree of hydration of ACC is high and a significant amount of water is mobile, water can be removed relatively easily.[64,78,102,109] With progressing dehydration, the interactions between water and ions contained in ACC become stronger such that the energy barrier for further water removal increases.[78] For example, when the degree of hydration decreases from 1.4 to 1, the activation energy barrier for dehydration increases from 50 kJ/mol to 120 kJ/mol, as shown in Figure 7B.[65] When the degree of hydration reaches values below the percolation threshold, *n*=0.8, the activation energy for further water removal increases even more rapidly.[79] This strong increase in the activation energy might be related to the need for substantial ion re-arrangements required to remove additional water.[30,79,100] For example, when *n* is around 0.2, where the majority of water is rigid[30,64,111] and hence strongly bound,[64,78,88,117] the activation energy for water removal is as high as 250 kJ/mol.[65] Once the activation energy for the removal of the remaining water is overcome such that ACC is fully dehydrated, crystalline $CaCO_3$ nuclei form and grow by consuming the amorphous matrix.[30] These results suggest that the kinetics of the solid-state transformation depend on the ion-water interactions within ACC and hence, on the ratio of mobile to rigid water contained in it.

The free energy of ACC particles decreases with increasing degree of hydration such that their thermodynamic stability increases.[79] However, the stability of ACC particles against crystallization, typically expressed as their lifetime or the critical

crystallization temperature or pressure, refers to their *kinetic* rather than their thermodynamic stability. These two stabilities are not directly related to each other: For example, the enthalpy of ACC particles increases with increasing pH of the solution they are synthesized from, such that their thermodynamic stability decreases.[20] Nevertheless, their kinetic stability, measured as the critical crystallization temperature, increases.[20]

The kinetic stability of ACC against a solid-state transformation is determined by the activation energy of its dehydration. With increasing degree of hydration, the mobility of ions increases, thereby facilitating their re-arrangement and reducing this activation energy.[79] Hence, the kinetic stability of ACC particles against solid-state transformation decreases with increasing degree of hydration,[29,30,111,115] as exemplified by the lower pressure required to induce their solid-state crystallization: ACC particles containing 10 wt% H_2O crystallize if loaded with 800 MPa, whereas those containing 21 wt% H_2O already crystallize if subjected to 240 MPa.[115]

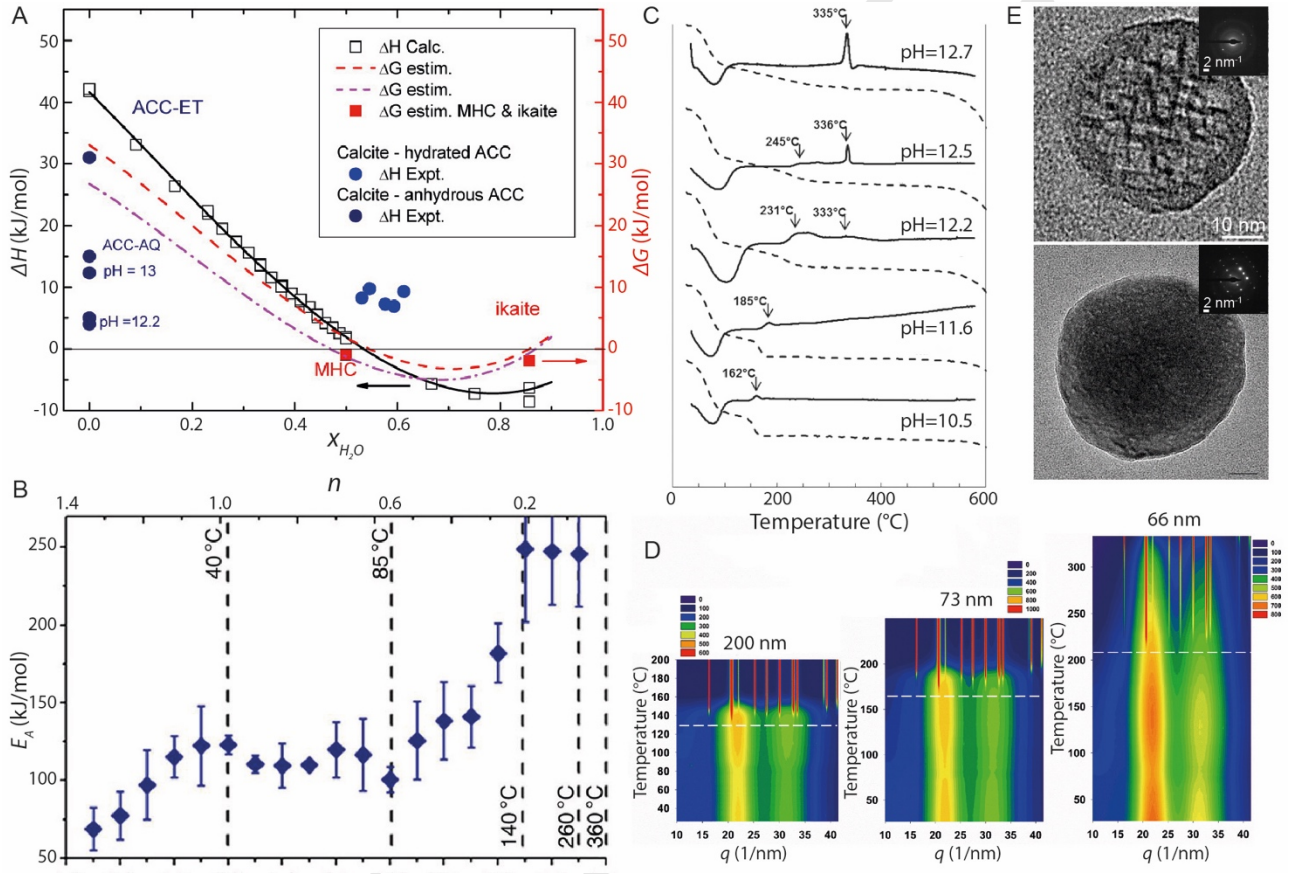

Figure 7. Solid-state transformation of ACC. (A) Enthalpy (left) and free energy (right) of ACC particles relative to calcite as function of the molar fraction of water (X_{H2O}) contained in ACC obtained by MD simulations.[79] (B) Activation energies (E_A) of the dehydration process of ACC as function of its degree of hydration (n).[65] C) DSC (solid line) and TGA (dashed line) analysis of ACC particles synthesized at different pHs.[86] (D) Contour plots of the wide-angle X-ray scattering (WAXS) intensity of ACC particles with different sizes while being heated as a function of the scattering vector (q) and temperature. When the solute concentration increases from 5 mM to 100 mM, the average diameter of the resulting ACC particles decreases from 200 nm to 66 nm. The critical crystallization temperatures are indicated by the white dashed lines.[69] (E) TEM images and SAED patterns of two ACC particles with different diameters after they have been transformed into crystals through annealing at 370℃ for 3 hours. Particles with diameters of 45 nm encompass nearly no mobile water whereas the molar ratio of mobile to rigid water in 130 nm diameter ACC particle is around 1.[30] Figures reproduced with permission from the American Chemical Society[30,69,79,86] and Springer Nature.[65]

The kinetic stability of ACC particles against solid-state transformation also depends on their synthesis conditions such as the pH and solute concentration.[20,86,100] For example, if the pH of the synthesis solution increases from 10.6 to 12.7, the kinetic stability of the resulting ACC particles, measured as their critical crystallization temperature, increases from 162 °C to 335 °C, as shown in Figure 7C.[86] Similarly, if the concentration of solutes present during the ACC synthesis increases from 5 mM to 100 mM, the critical crystallization temperature of the resulting ACC particles increases from 130 °C to 220 °C, as shown in Figure 7D.[69] This increase in kinetic stability was assigned to a decrease in the particle size: As the pH or solute concentration increase, the degree of supersaturation of the solution increases such that ACC particles with smaller sizes are produced.[69] The surface energy of ACC is below that of any of the crystalline counterparts, such that smaller ACC particles, that have a higher surface-to-volume ratio, are thermodynamically more stable than larger ones.[69] However, it is unlikely that the higher kinetic stability of smaller ACC particles is related to their higher thermodynamic stability. Instead, these small ACC particles display a different dehydration behavior than larger particles that have a similar degree of hydration.[69] This observation suggests that the ratio of rigid to mobile water is a function of the particle size and that this ratio influences the kinetic stability of ACC against solid-state transformation.

The structure of $CaCO_3$ crystals can be controlled with the kinetics of the solid-state transformation and hence, with external crystallization triggers. If ACC particles undergo a fast solid-state transformation, for example induced by subjecting them to high temperatures, they transform into the thermodynamically most stable polymorph, calcite.[69,84,111] By contrast, if the solid-state transformation is slower, for example if ACC is exposed to elevated pressures, a mixture of calcite and metastable vaterite forms.[115,116] The fraction of vaterite present in this mixture increases with decreasing pressure, that most likely decreases the rate of the solid-state transformation.[115] Not only the structure, but also the crystallite size can be tuned with the transformation kinetics: If the ratio of mobile to rigid water contained in ACC increases such that the transformation kinetics becomes faster, the crystallite size increases, as shown in Figure 7E.[30]

4.2. Dissolution-recrystallization

If ACC particles are exposed to bulk aqueous solutions, they tend to dissolve. The resulting solutions become supersaturated with respect to the crystal phase and $CaCO_3$ crystals start form.[69,111] This mechanism has been extensively studied using different techniques such as X-ray microscopy,[42] time-resolved small- and wide-angle X-ray scattering,[22] titration,[69] electron microscopy,[29] and isotope tracing.[118] It is typically referred to as dissolution-recrystallization albeit $CaCO_3$ crystals never formed before. Nevertheless, to be consistent with most literature, we use this expression in this review.

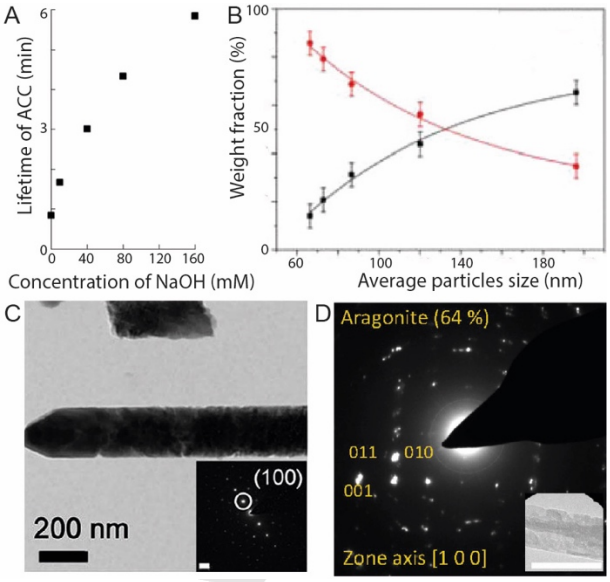

Figure 8. Crystallization of ACC through the dissolution-recrystallization mechanism. (A) Influence of the NaOH concentration on the lifetime of ACC dispersed in aqueous solutions.[86] (B) Weight fraction of calcite (black) and vaterite (red) formed from ACC particles dispersed in an aqueous solution as a function of the ACC particle size.[69] (C, D) TEM images and SAED patterns of single-crystalline (C) vaterite[119] and (D) aragonite[120] nanowires formed within track-etched nanopores. Figures reproduced with permission from the American Chemical Society,[69,86] the Royal Society of Chemistry,[119] and the National Academy of Sciences.[120]

If ACC particles are in contact with bulk water, their kinetic stability is primarily determined by the dissolution rate of ACC particles and the nucleation and growth of new crystals. It has been suggested that the dissolution of ACC particles at room temperature is preceded by their dehydration.[21,29,43,65,113,114] However, the very high activation energies of the ACC dehydration, that range from 50 to 250 kJ/mol,[65] kinetically hinder this process such that it is questionable if ACC particles dehydrate before they dissolve in bulk water. According to the Noyes-Whitney equation,[121] the dissolution rate can be expressed as

$$r = A\frac{D}{d}(C_s - C_b)$$

where r is the dissolution rate, A the surface area of ACC particles, d the distance over which Ca^{2+} and CO_3^{-2} ion concentration gradients exists, D the diffusion coefficient of ions, C_s the saturation concentration of ions with respect to the solubility of ACC, and C_b the concentration of ions in bulk solutions. These parameters and hence the dissolution kinetics can be influenced by the size[69] and degree of hydration[29] of ACC particles as well as the crystallization conditions such as the pH,[49,122] temperature,[25,57] and solvent[82,123,124] of the ACC encompassing solution. For example, if the ethanol volume fraction in the solution increases from 76 vol% to 98 vol%, the time required to dissolve ACC particles and form crystals increases from 1.5 h to 4 days.[123] If all the water is replaced by ethanol, the crystallization time even increases to 7 days.[124] Similarly, ACC particles with smaller sizes, that are produced from solutions possessing a higher degree of supersaturation, display an increased ACC dissolution rate

compared to larger counterparts.[69,125] As a result, the kinetic stability of small particles in bulk solutions is lower than that of bigger ones.[69] Remarkably, the kinetic stability of ACC particles increases with increasing pH of the synthesis solution[86,124] although their solubility increases[49,122,126] and their size decreases,[69] as shown in Figure 8A. This increase in the kinetic stability likely is related to the high concentration of hydroxide ions, present at high pHs that slows down the formation of new crystals.[86] These examples illustrate that the kinetic stability of ACC against dissolution and the formation of $CaCO_3$ crystals is a complex interplay between multiple factors. Further studies are warranted to relate the influence of the different synthesis conditions to the dissolution of ACC particles as well as the nucleation and growth of new crystals.

The structure of $CaCO_3$ crystals that form from solutions containing ACC particles is primarily governed by the kinetics of their dissolution and that of the crystal formation.[29,69,118] The dissolution kinetics influences the local degree of supersaturation with respect to one of the crystalline $CaCO_3$ polymorphs. Hence, it also influences the kinetics of nucleation and growth of new crystals.[69,122,124] For example, within the same observation time, small ACC particles that quickly dissolve preferentially transform into vaterite whereas larger ACC particles that dissolve more slowly tend to transform into the calcite, as shown in Figure 8B.[69] However, if ACC particles are left in solution for an extended amount of time, the final crystals always attain the thermodynamically most favorable structure, calcite.[21,43,86]

The kinetic stability of ACC in bulk solutions can be enhanced if the solution is confined. This is the case, for example, if ACC particles are contained in aqueous cores of 50 nm to 1 μm diameter liposomes,[83,127,128] 50 nm to 200 nm diameter rod-shaped pores of track-etched membranes,[26] or 4-10 μm diameter drops deposited onto self-assembled monolayers.[129] The confined volume restricts the transport of dissolved ions away from the ACC surface thereby slowing down the dissolution of ACC[129] as well as the nucleation and growth of new crystals.[130] A slower crystallization enables arresting crystals in a metastable form that displays an unusual morphology. For example, if ACC is contained in track-etched nanopores, it can transform into single-crystalline vaterite[119] and aragonite[120] nanowires with well-defined diameters, as shown in Figures 8C and D. Hence, confinement can offer control over the morphology and structure of $CaCO_3$ crystals.

If ACC particles are exposed to humid air, they also crystallize through a dissolution-recrystallization pathway: Water contained in the air adsorbs at the surface of ACC particles and dissolves them such that crystals start to form from a supersaturated solution.[29,111,112] Because the dissolution kinetics of ACC particles scales with the rate of water adsorbed at their surface, their kinetic stability decreases with increasing humidity.[111,112] For example, if ACC particles are stored at a relative humidity of 35%, they are stable against crystallization for more than 4 hours whereas they crystallize within 1 hour if the relative humidity is increased to 90%.[111] Similarly, the crystallization kinetics increases with increasing degree of hydration of the ACC.[74,108] For example, if ACC particles are freeze dried to remove the mobile water contained in them and stored under reduced pressures or in gastight vials, they remain amorphous for more than 150 days.[112] The much lower amount of water available to dissolve ACC also delays the crystallization kinetics of $CaCO_3$: If transformed under these conditions, metastable crystalline phases, such as aragonite can form; these metastable polymorphs do not form in bulk solutions at room temperature in the absence of any additive.[112]

5. Additives

Most ACC found in nature contains various soluble additives, such as Mg^{2+}, and acidic proteins containing carboxyl or phosphate groups.[9] These additives influence the formation[131–133] of ACC, its structure,[9,96,97] and stability[74,123,134,135] as well as the composition, morphology, structure, and mechanical properties of the resulting crystals.[4,6,136,137] Inspired by nature, additives have been extensively used to tune the formation of $CaCO_3$ and thereby the properties of synthetic $CaCO_3$-based materials.[26,33,120,138,139,139–144] Some of the influences of the most commonly employed additives are summarized below.

5.1. Mg^{2+}

If ACC is formed from a highly supersaturated solution containing Ca^{2+}, CO_3^{2-}, and Mg^{2+} ions, an ACC phase encompassing Mg^{2+} (Mg-ACC) phase usually precipitates first.[145–150] The formation of Mg-ACC is thermodynamically favored over that of pure ACC[151] because the charge density of Mg^{2+} is higher than that of Ca^{2+},[152,153] such that the Mg-ACC phase more strongly interacts with water.[154] This strong interaction increases the amount of water contained in the amorphous phase[135,155] such that the free energy of Mg-ACC is lower compared to pure ACC. However, the kinetics of the nucleation and growth of Mg-ACC is not significantly affected by the incorporation of Mg^{2+}[156] such that the size of Mg-ACC particles is similar to that of pure ACC ones.[74,157] The composition of the Mg-ACC phase, namely the amount of Mg^{2+} that is incorporated into it, depends on the solute concentration,[158] and the solution pH.[159] In addition, the amount of incorporated Mg^{2+} depends on the ratio of Mg^{2+}:Ca^{2+} contained in the solution.[145,147,158,159] Nevertheless, the Mg addition is not stochiometric but the ratio of Mg^{2+}:Ca^{2+} in Mg-ACC particles is always below that of the solution they are produced from. The preferential incorporation of Ca^{2+} into the amorphous phase might be caused by the slow dehydration kinetics of Mg^{2+} ions that delays their inclusion.[151,160] In line with this hypothesis, the incorporation kinetics and hence, the fraction of incorporated ions increases with increasing radii of divalent cations such that the incorporation efficiency into ACC increases from Mg^{2+} to Sr^{2+} to Ba^{2+}.[157]

Due to the difference in the ionic radii of Ca^{2+} and Mg^{2+}, the structure of ACC changes upon addition of Mg^{2+}. The average *CN* and *R* of the first Ca-O coordination shell of Mg-ACC has been reported to be distinctly different from that of pure ACC, as determined with Ca K-edge EXAFS.[98] This is in contrast to more recent ^{43}Ca NMR[101] and ^{13}C NMR[159] studies that provide no

evidence for any change in the short-range order of ACC around Ca atoms upon incorporation of Mg^{2+}. Indeed, PDF analysis suggests that the structure of Mg-ACC is a mixture of pure ACC and pure amorphous magnesium carbonate (AMC) nanoclusters, as shown in Figure 9A.[151] If the molar faction of Mg^{2+} is below 0.48, ACC and AMC nanoclusters are homogeneously distributed within the amorphous particles.[151,159] Their distribution must be further assessed if the Mg^{2+} molar fraction is higher.[151,159] Magnesium ions are often employed to increase the stability of ACC against crystallization in bulk solutions. Indeed, the lifetime of Mg-ACC particles increases with increasing molar fraction of Mg^{2+} in solution that can lead to an increased concentration of Mg^{2+} in Mg-ACC, as shown in Figure 9B.[145,147] The increased lifetime of Mg-ACC has been related to its reduced free energy compared to pure ACC.[151] However, the lifetime of ACC is solely related to the dissolution and crystallization kinetics and hence, it is in a first approximation independent of the thermodynamic stability of these particles. Indeed, the lifetime of AMC is longer than that of ACC, despite of its lower thermodynamic stability.[151] The observed increased lifetime of Mg-ACC has been related to the higher dehydration energy of Mg^{2+} compared to that of Ca^{2+} that slows down the dehydration of the amorphous phase prior to its crystallization.[103,151,161,162] However, the high activation energy associated with the dehydration kinetically hinders this process such that it is unlikely to occur in the presence of bulk water at room temperature. Instead, Mg-ACC particles that are in contact with bulk water dissolve and new crystals forms from the supersaturated solution.[118] In this case, the observed delay in the crystallization of Mg-ACC must be related to its retarded kinetics of dissolution and the delayed nucleation and growth of new crystals. This delay must be caused by Mg^{2+} ions present in Mg-ACC as well as in the bulk solution. The lower free energy of Mg-ACC is expected to reduce its solubility in aqueous solutions,[29,151] thereby slowing down its dissolution. However, this expectation could experimentally not been confirmed: the dissolution profiles of pure ACC and Mg-ACC are very similar if particles are dispersed in pure water.[135] Remarkably, the addition of small amount of free Mg^{2+} ions significantly delays the dissolution of pure ACC particles.[154] These results indicate that the dissolution kinetics is mainly influenced by free Mg^{2+} ions present in bulk solutions rather than those contained in Mg-ACC. Free Mg^{2+} ions can also influence the growth kinetics of new crystals: These ions can adsorb onto the surfaces of newly formed crystals, thereby delaying or even inhibiting their growth.[38] Hence, the crystallization kinetics of the amorphous phase can be slowed down by free Mg^{2+} ions.[135,145] As a result of the delayed crystallization kinetics of Mg-ACC particles observed in the presence of free Mg^{2+} ions, these particles are more stable against crystallization than pure ACC ones not only in bulk solutions but also if stored in a humid environment, as shown in Figure 9C.[74,149,151,158]

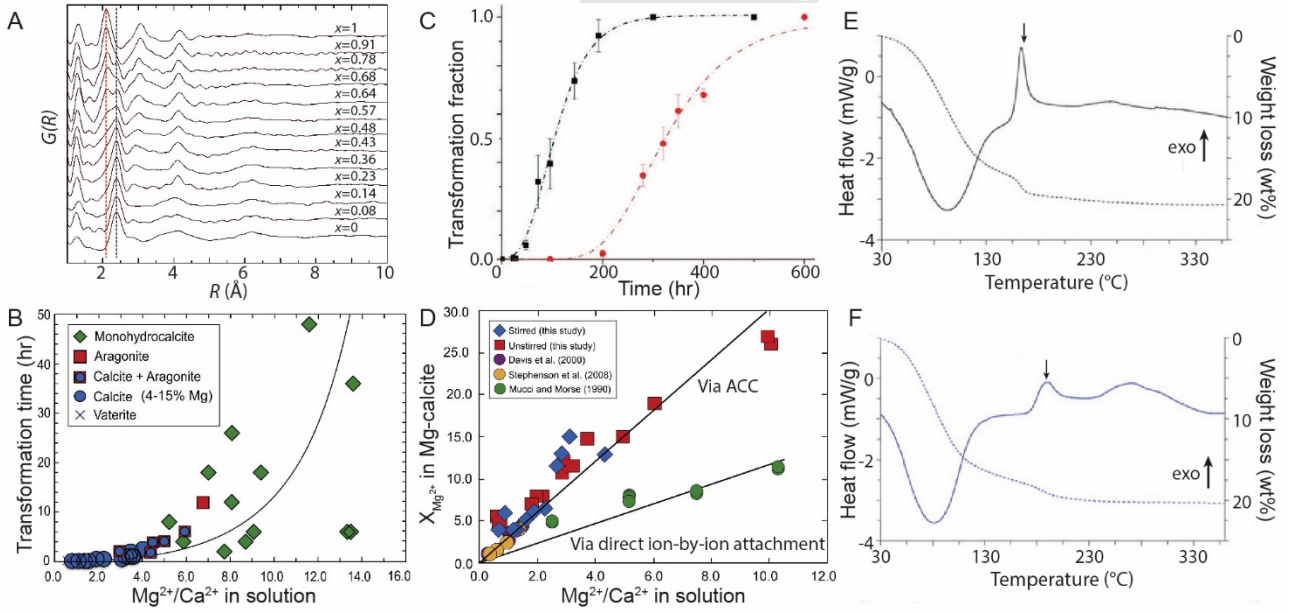

Figure 9. Influence of Mg^{2+} ions on the formation of $CaCO_3$. (A) PDFs of the Mg-ACC ($Ca_{1-x}Mg_xCO_3 \cdot nH_2O$) with different molar fractions of incorporated Mg^{2+} ions (x). The first Mg-O coordination shell is indicated with the red line and the first Ca-O coordination shell with the black line. Their peak positions are independent of x, indicating that there is no change in the short-range order around Ca or Mg atoms upon incorporation of Mg^{2+} ions into ACC.[151] (B) Influence of the Mg^{2+}:Ca^{2+} molar ratio in the aqueous solutions on the kinetic stability of Mg-ACC particles against transformation into different crystalline $CaCO_3$ polymorphs.[147] (C) Evolution of the crystallization of pure ACC (black) and Mg-ACC (red), synthesized from a solution containing a molar ratio of Mg^{2+}:Ca^{2+} of 0.1, as function of time when stored in humid air (RH≈ 50%).[149] (D) Influence of the molar ratio of Mg^{2+}/Ca^{2+} ions in solution on the molar fraction of Mg^{2+} (X_{Mg2+}) incorporated in the resulting Mg-calcite crystals formed through ion-by-ion attachment and from Mg-ACC precursors. The molar fraction of Mg^{2+} ions present in the resulting Mg-calcite are approximately three-fold lower if produced through ion-by-ion attachment in the absence of Mg-ACC precursors.[147] (E, F) DSC (solid line) and TGA (dashed line) analysis of (E) pure ACC and (F) Mg-ACC that contains 2.4 mol% Mg^{2+}. The critical crystallization temperatures are marked with arrows.[74] Figures reproduced with permission from Elsevier,[147,151] the Royal Society of Chemistry,[149] and John Wiley & Sons.[74]

Additives such as Mg^{2+} influence the crystallization kinetics of ACC in the presence of bulk water. In addition, they affect the structure of the resulting crystals. If the ratio of Mg^{2+}:Ca^{2+} in the aqueous solution is high, Mg-ACC preferentially transforms into aragonite or monohydrocalcite, as shown in Figure 9B.[145,147] By contrast, if the Mg^{2+}:Ca^{2+} ratio is low, Mg-ACC preferentially transforms into Mg-calcite.[145,147] Remarkably, the molar fraction of Mg^{2+} contained in Mg-calcite crystals is always identical to that in Mg-ACC precursors.[147] This good correlation suggests that Mg-ACC particles strongly influence the formation of Mg-calcite. Their influence most likely is related to the ratio of Mg^{2+}:Ca^{2+} ions present in the locally supersaturated solution that scales with that of dissolved Mg-ACC particles.[147] By contrast, if Mg-calcite is produced from solutions that are supersaturated relative to calcite, Mg-calcite directly forms through ion-by-ion attachment without the formation of any Mg-ACC intermediates. In this case, the molar fraction of Mg^{2+} in Mg-calcite is approximately three-fold reduced compared to that in particles produced via Mg-ACC precursors, as shown in Figure 9D.[147] This comparison demonstrates that higher amounts of Mg^{2+} can be incorporated into Mg-calcite particles if they form through the dissolution-recrystallization of Mg-ACC. The amount of incorporated Mg^{2+} influences the properties of Mg-calcite crystals and hence, is an important parameter that needs to be closely controlled if materials with well-defined properties want to be synthesized.[145,148,149,163,164]

The incorporation of magnesium ions into ACC also delays its solid-state transformation: The strong interactions between Mg^{2+} and water molecules reduce the mobility of water,[155,160,165] thereby increasing the fraction of rigid water contained in Mg-ACC compared to that contained in ACC.[155] As a result of this stronger interactions, the activation energy for the dehydration of Mg-ACC is higher than that of pure ACC such that the temperature where Mg-ACC starts to crystallize is higher.[74,135] For example, ACC containing 2.4 mol% Mg^{2+} starts to crystallize around 190 °C, while pure ACC crystallizes around 160 °C, as shown in Figures 9 E and F.[74] Despite of the different crystallization temperatures, the structure of the resulting crystals is usually the same: calcite.[74,135]

5.2. Other low molecular weight additives

Many other low molecular weight additives as well as phosphates and sulfates are well-known to influence the ACC formation. These additives typically contain functional groups that display a high affinity to Ca^{2+}.[131,132] For example, citrate, that contains carboxylic groups, has been reported to favor the formation and stabilization of $CaCO_3$ PNCs, thereby delaying the nucleation of ACC particles.[131,132] Yet, this additive does not change the critical degree of supersaturation such that it does not noticeably influence the size of the resulting ACC particles.[166] A similar behavior has been observed for other carboxyl-containing molecules such as aspartic acid and glycine.[157,167]

Atomic absorption spectroscopy (AAS), TGA, and X-ray photoelectron spectroscopy (XPS) suggest that carboxy-containing low molecular weight additives are contained within the ACC particles or associated with their surfaces.[135,166,167] By contrast, amino acid analysis did not reveal any traces of aspartic acid within ACC particles.[157] These results imply that aspartic acid is preferentially adsorbed at the surface of particles from where it can be removed by thoroughly washing them. This implication is supported by PDF analysis that does not reveal any significant structural difference of ACC particles upon their functionalization with aspartic acid, glycine, or citric acid.[166,167] However, to conclusively determine the location of low molecular weight additives that are associated with ACC particles, further studies are warranted.

Phosphates display a distinctly different behavior: They favor the formation of $CaCO_3$-rich liquid phases during the liquid-liquid phase separation or stabilize these phases once they formed.[132,157] Thereby, these additives increase the critical supersaturation concentration where nucleation of ACC occurs,[131,132] such that much smaller ACC particles form.[74,157] Based on FTIR and ^{31}P solid-state NMR analysis, it has been suggested that phosphate ions are molecularly dispersed in the resulting ACC particles.[157,168] However, these additives do not significantly influence the short- and medium-range order of ACC. The only slight structural difference that could be observed with PDF was a broadening of the peak around 4.1 Å.[74] Many low molecular weight additives that possess a high affinity to Ca^{2+} increase the kinetic stability of ACC particles if dispersed in bulk solutions, as shown in Figure 10A.[135] In particular, phosphates,[74] sulfates,[135] and carboxy-containing molecules including citrate,[166] phytic acid,[169] and amino acids such as glycine,[167] aspartic acid,[135,167] phosphor-serine,[170] and phosphor-threonine[170] have been reported to strongly increase the lifetime of ACC particles. The increased kinetic stability of these particles must be related to a delayed dissolution of ACC or a retarded formation of $CaCO_3$ crystals. The influence of low molecular additives on the dissolution rate of ACC particles remains unclear. By contrast, many of these additives, including phosphates,[171,172] sulfates,[21,172] citrate,[172] and aspartic acid[173,174] are known to slow down or even inhibit the growth of crystals by adsorbing on their surfaces. Indeed, the kinetic stability of ACC against crystallization in the presence of bulk water increases with increasing ability of these additives to inhibit crystal growth. As a result of this correlation, the stability of ACC particles sequentially increases if functionalized with valine, asparagine, glutamic acid, and aspartic acid due to their increasing affinity towards the $CaCO_3$ crystal surface, as shown in Figure 10B.[175]

Certain low molecular weight additives also delay the crystallization of ACC particles that are not in contact with bulk water and hence undergo a solid-state transformation. These additives do not significantly change the structure or overall degree of hydration of ACC.[74,135,157,166,167] Instead, they strongly interact with water contained in ACC, thereby reducing its mobility and hence increasing the energy barrier for dehydration.[74,166,168] Therefore these additives enhance the stability of ACC against solid-state transformation such that the temperature required to initiate crystallization is significantly higher.[74,135,166,168] For example, pure ACC transforms into calcite at 160 °C, whereas ACC particles that are synthesized in the presence of 35 mol% citrate only crystallize at 329 °C, as shown in Figure 10C.[166]

Similar increases in the critical crystallization temperature have been reported for ACC particles functionalized with phosphate[168] and aspartic acid.[135]

Certain low molecular weight additives not only increase the stability of ACC, but also influence the size, structure, morphology, and properties of the resulting $CaCO_3$ crystals. For example, if high concentrations of citrates are present in bulk solutions, ACC preferentially transforms into the stable calcite rather than the metastable vaterite phase because citrates delay or even inhibit the growth of vaterite.[166,176] As the citrate concentration increases, the size of the final calcite crystals decreases and their morphology changes from typical rhombohedra to elongated spheroids with rougher surfaces, as exemplified in the SEM images in Figure 10D.[166,176] Remarkably, some organic additives, such as aspartic acid or glutamic acid with a defined chirality can even control the chiral direction of spiraling vaterite crystals that form in their presence, as shown in Figure 10E.[177] Moreover, these low molecular weight additives can influence the mechanical properties of the resulting crystals: If 7 mol% glycine or 4 mol% aspartic acid are incorporated into calcite single crystals, their hardness increases two-fold, as shown in Figure 10F.[138]

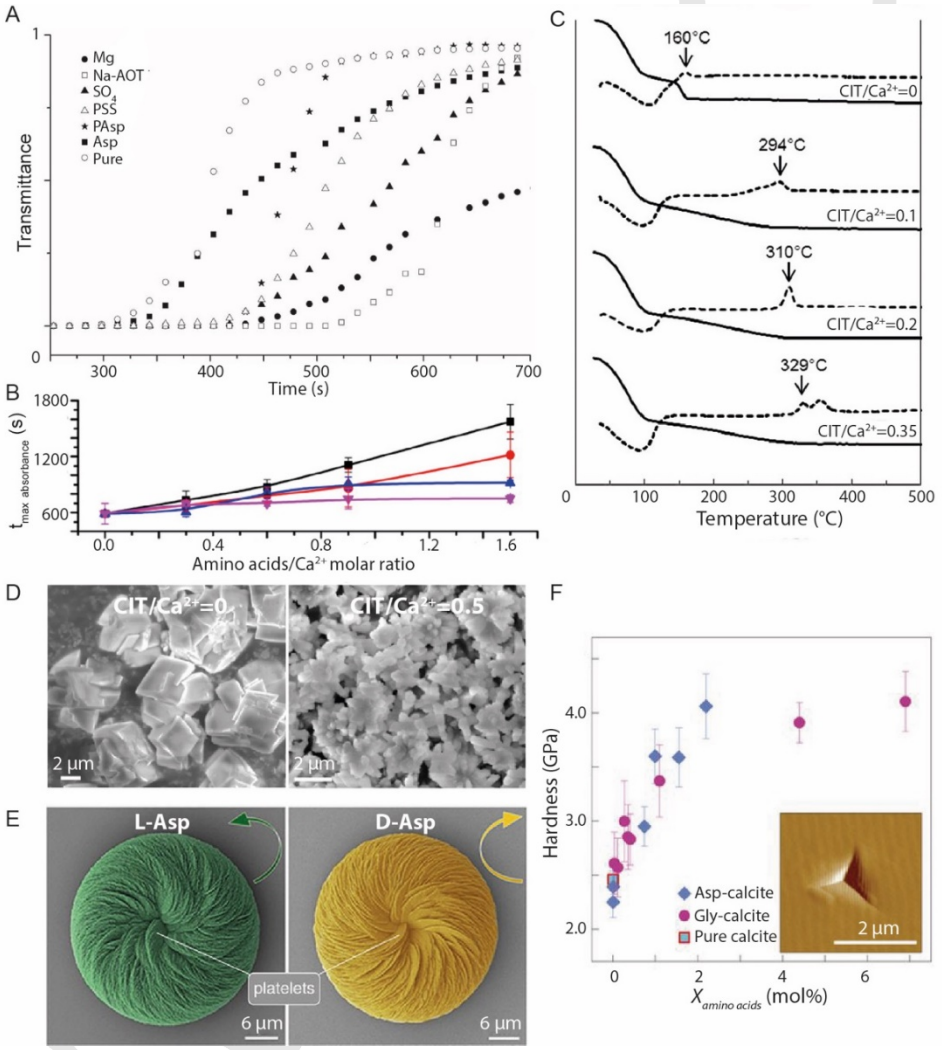

Figure 10. Influence of other low molecular weight additives on the formation of $CaCO_3$. (A) Evolution of the UV-vis transmittance recovery as a function of time after an aqueous solution containing 1 M $CaCl_2$ is mixed with one containing 1 M Na_2CO_3 in the presence of 200 ppm poly(styrene sulfonate) (PSS), aspartic acid (Asp), poly(aspartic acid) (PAsp), bis(2-ethylhexyl)sulfosuccinate (AOT), 10 mM Mg^{2+}, or 2 mM SO_4^{2-}.The longer the recovery time of the transmittance is, the higher is the kinetic stability of ACC particles against crystallization in bulk solutions.[135] (B) Influence of the molar ratio of amino acids:Ca^{2+} on the lifetime of ACC particles dispersed in an aqueous solutions, measured as the time where the maximum absorbance appears in turbidimetric analysis, for aspartic acid (black), glutamic acid (red), asparagine (blue), and valine (pink).[175] (C) TGA (solid line) and DSC (dashed line) analysis of ACC particles synthesized in the presence of different amounts of citrate (CIT). The critical crystallization temperatures are marked with arrows.[166] (D) SEM images of calcite crystals formed from ACC particles in the presence of different amounts of citrate. The CIT/Ca^{2+} molar ratios are indicated in the SEM images.[166] (E) SEM images of toroid vaterite crystals formed in the presence of L-aspartic acid that spiral counterclockwise (green) and D-aspartic acid that spiral clockwise (yellow).[177] (F) Influence of the molar fraction of aspartic acid (blue) and glycine (pink) that are incorporated into calcite single crystals on their hardness. A scanning force microscopy image showing the plastic deformation of additive-functionalized calcite is shown in the inset.[138] Figures reproduced with permission from John Wiley & Sons,[135,166] the American Chemical Society,[175] and Springer Nature.[138,177]

5.3. High molecular weight organic additives

The formation of ACC can also be influenced by certain high molecular weight organic additives. By analogy to the influential low molecular weight additives, these polymeric additives possess functional groups with a high affinity to Ca^{2+}. A prominent example is poly(acrylic acid) (PAA) that strongly interacts with Ca^{2+} ions, thereby decreasing the degree of supersaturation of the solution and hence delaying the nucleation of ACC.[131] Sulfonate groups have a lower affinity towards Ca^{2+} than carboxylic groups such that the influence of sulfonate-containing additives such as PSS on the ACC formation kinetics[132] and their stability against crystallization[123] is weaker than that of carboxy-containing counterparts, such as PAA. The attractive interaction between these additives and Ca^{2+} also leads to the formation of additive-Ca^{2+} complexes with a well-defined morphology. For example, the presence of PAA in Ca^{2+} containing solutions leads to the formation of crosslinked Ca-PAA polymer networks, as shown in Figure 11A.[42] Similarly, the presence of PSS in Ca^{2+} containing solutions leads to the formation of spherical globules, as shown in Figure 11B.[32] These complexes can also restrict the ion transport, thereby delaying the formation of ACC.[42]

Certain high molecular weight organic additives, such as poly(aspartic acid) (PAsp),[33,61] poly(arginine),[157] poly(allylamine hydro-chloride),[178] and ovalbumin[62] not only interact with Ca^{2+} or CO_3^{2-} ions but also induce the formation of $CaCO_3$-rich liquid phases or stabilize these phases after they formed. In addition, these and many other high molecular weight additives containing multiple charged groups delay the ACC formation through one or a combination of these mechanisms.[132,179–181] Most of them also reduce the size of the forming ACC particles.[42,123,182,183]

High molecular weight additives are too big to be incorporated into ACC particles, such that they usually adsorb on their surfaces.[32,42,72,182] Hence, they can also be added after ACC particles are synthesized. Indeed, it has been demonstrated that PAsp stabilizes ACC particles more efficiently against crystallization if it is added to the suspension after the ACC particles have been synthesized.[182] In both cases, the kinetic stability of ACC particles against dissolution-recrystallization increases with the concentration of high molecular weight additives present in the solution during their synthesis.[42,50,182] The resulting additive shells delay or even inhibit the ACC dissolution, if they are in contact with bulk water.[42,50] They also hinder the diffusion of ions from the dissolving ACC particles to the forming $CaCO_3$ crystals, thereby retarding their growth.[32,182] Similar delays in the crystallization of ACC particles are observed if they are coated with an inorganic shell, silica, as shown in Figure 11C.[65,184] Moreover, the growth of the $CaCO_3$ crystals can be further slowed down if certain organic additives, such as PAsp,[185] that display high affinities to the crystal surfaces are present. These results indicate that certain high molecular weight additives stabilize ACC particles by reducing the kinetics of the dissolution-recrystallization process.

Some high molecular weight additives also influence the structure, size, and morphology of the resulting $CaCO_3$ crystals. For example, at low concentrations, PAsp promotes the formation of calcite.[182] With increasing PAsp concentration, the size of calcite crystals decreases and their morphology changes from typical rhombohedra that possess smooth facets to those with rounded and rough surfaces.[185] If the PAsp concentration is further increased, vaterite forms.[182] A similar effect on the morphology of calcite is observed in the presence of PSS: At high PSS concentrations, faces of the calcite crystals, that are typically flat, become concave, as shown in Figure 11D.[186,187]

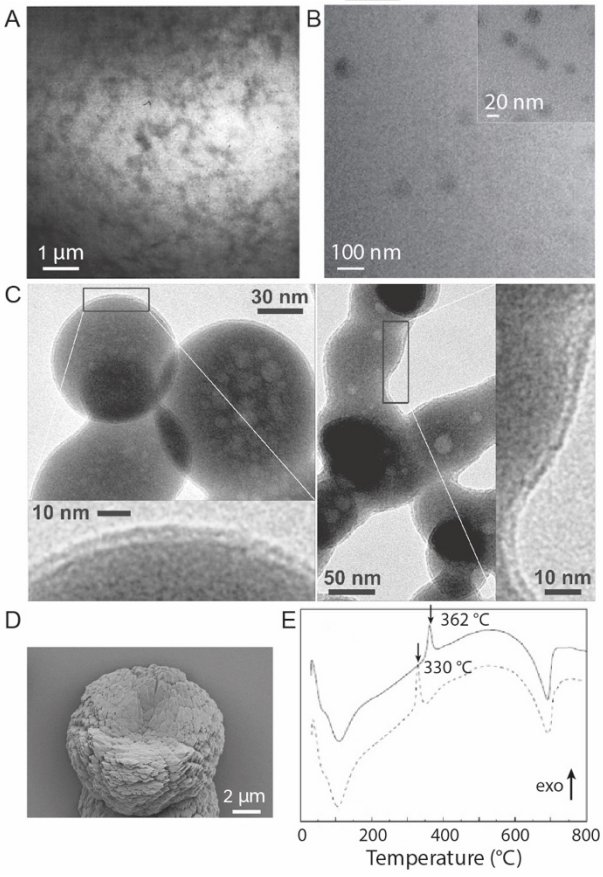

Figure 11. Influence of high molecular weight organic additives on the formation of $CaCO_3$. (A) X-ray microscopy image of Ca-PAA complexes.[42] (B) TEM images of Ca-PSS globules.[32] (C) TEM images of ACC particles coated with a silica shell.[184] (D) SEM image of a calcite crystal synthesized from an aqueous solution containing 5 mM Ca^{2+} ions in the presence of 0.5 g L^{-1} PSS displaying a concave surface.[186] (E) DSC analysis of PSS-functionalized ACC particles that are synthesized in solutions encompassing a molar ratio of PSS:Ca of 1:4 (solid line) and 1:32 (dashed line). The critical crystallization temperatures are marked with arrows.[123] Figures reproduced with permission from the American Chemical Society,[42,184] Springer Nature,[32] John Wiley & Sons,[186] and Elsevier.[123]

Certain high molecular weight additives also influence the kinetic stability of ACC against solid-state transformation. These additives typically possess a high affinity towards water and hence, reduce the mobility of water associated with ACC,[30] even though they do not significantly change its hydration.[123,135,157,182] As a result of the reduced water mobility, the temperature required to induce a solid-state transformation of ACC is markedly increased. For example, the critical crystallization temperature of

ACC particles increases from 277 °C to 362 °C if they are synthesized from a bulk solution containing a PSS : Ca ratio of 1:4, as shown in Figure 11E.[123] Similarly, the crystallization temperature of PAA-functionalized ACC particles increases with increasing amount of PAA added during their synthesis.[123]

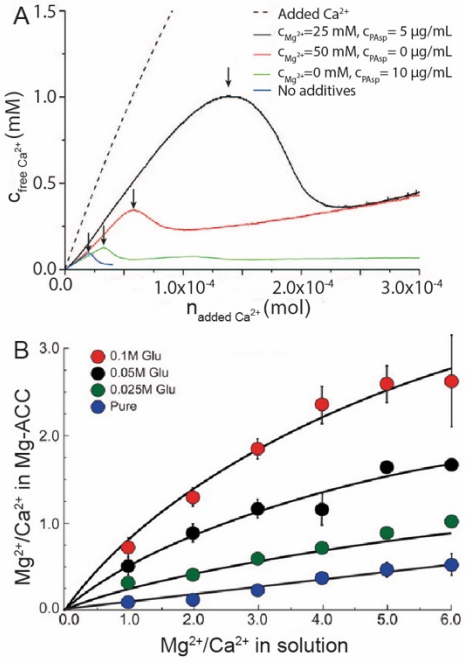

Figure 12. Synergic effects of multiple types of additives on the formation and composition of ACC. (A) Evolution of the concentration of free Ca^{2+} ions in a carbonate-buffered solution (pH = 9.75) upon continuous addition of a $CaCl_2$-containing solution that does not contain any additives (blue), contains PAsp (green), Mg^{2+} (red), or PAsp and Mg^{2+} (black). The total concentration of Ca^{2+} ions added to the solution is indicated by the dashed line. The points where ACC starts to form are marked with arrows.[188] (B) The molar ratio of Mg^{2+}:Ca^{2+} in Mg-ACC as function of the molar ratio Mg^{2+}:Ca^{2+} in a solution that does not contain any additional additives (blue), contains 0.025 M glutamic acid (green), 0.05 M glutamic acid (black), or 0.1 M glutamic acid (red).[189] Figures reproduced with permission from the Royal Society of Chemistry[188] and the National Academy of Sciences.[189]

In summary, many additives strongly influence the formation of ACC and hence, its structure, hydration, and stability against crystallization. These additives also influence the size, structure, and morphology, and hence, the properties of the forming $CaCO_3$ crystals. If multiple types of additives are simultaneously present during the crystallization of $CaCO_3$, an even closer control over the crystallization process can be achieved. For example, the formation of ACC is delayed more efficiently if Mg^{2+} is added to PAsp-containing solutions that are supersaturated with respect to ACC, as shown in Figure 12A.[188],[59] Similarly, the amount of Mg^{2+} that is incorporated in Mg-ACC and hence, also in Mg-calcite, increases if certain low molecular weight carboxyl-containing additives are present during its synthesis, as shown in Figure 12B.[189] The increased Mg^{2+} concentration influences the mechanical properties of Mg-calcite.[164,190] A better understanding of potential synergic effects of different additives on the composition, structure, hydration, and stability of ACC would further our understanding on the $CaCO_3$ crystallization in nature. This understanding would offer a superior control over the crystallization process and hence the properties of the resulting $CaCO_3$-based materials.

6. Conclusion

Nature produces $CaCO_3$–based functional materials that display a fascinating combination of properties. The unique control nature possesses over these properties is most likely related to the excellent control over the structure and local composition of $CaCO_3$ that is obtained by closely tuning the crystallization process, for example using soluble additives.[4–6] Even though a lot of excellent work has been performed to elucidate biomineralization processes, it is still not entirely clear how nature controls the formation of $CaCO_3$. This lack in our understanding is in parts related to the complex conditions under which nature produces these materials.[4,5] To gain a deeper understanding on the crystallization of $CaCO_3$ and thereby a better control over the formation of these materials, $CaCO_3$ has been synthesized in the laboratory by systematically varying synthesis conditions in the presence and absence of additives. These studies significantly furthered our understanding of the $CaCO_3$ formation. However, we are far from understanding the influence of all synthesis conditions and additives on the crystallization of $CaCO_3$ such that we cannot control its composition, structure, and morphology, and hence the properties of resulting $CaCO_3$–based functional materials to a similar extent as nature.

In natural and synthetic systems, $CaCO_3$ crystals typically form from ACC precursors. The formation of these amorphous precursors has been described with classical nucleation and growth models as well as with non-classical models. The exact mechanisms by which ACC forms are still debated, in parts because it is difficult to experimentally probe early stages of the $CaCO_3$ formation with a sufficiently high simultaneous temporal and spatial resolution.[47] Nevertheless, it is clear that water plays an important role in the different stages of $CaCO_3$ formation. Our understanding of the thermodynamic and kinetic roles of water in the formation of ACC, its structure and crystallization, has been rapidly expanded in the last decade. An important reason for this progress is the use of advanced experimental characterization techniques and MD simulations that offer insights into the $CaCO_3$ formation and crystallization with a much higher temporal and spatial resolution than was possible before. These studies reveal two types of water molecules that can be encompassed in ACC: mobile and rigid water. The ratio of mobile to rigid water is crucial to determine the short- and medium-range order of the structures of ACC and its kinetic stability against crystallization.

Many synthesis conditions such as the solute concentrations, pH, and temperature of the solution as well as the solvent choice have been shown to influence the formation of ACC particles, their structure, hydration, and crystallization kinetics. However, the exact reasons for this correlation between the synthesis conditions and the structure and properties of the forming $CaCO_3$ phases are, at least in parts, still unclear. Synthesis conditions likely influence the amount and type of water that is incorporated

in ACC and hence, its structure and stability against crystallization. These parameters have been shown to influence the structure of the final $CaCO_3$ crystals that form from ACC. Some similar effects can be achieved if the crystallization of $CaCO_3$ is controlled with certain additives. However, further studies on the influence of the synthesis conditions and additives on the formation of $CaCO_3$, including the amount and type of water contained in it are warranted to gain a more holistic understanding.

A cautiously chosen combination of additives offers an even better control over the crystallization process and hence, over the composition, morphology, structure, and properties of the forming $CaCO_3$ crystals than individual additives do. However, synergic effects of additives only start to be systematically explored, such that we currently cannot fully leverage this feature to the extent nature can. An improved understanding of these synergic effects that likely are also influenced by the synthesis conditions, would open up new possibilities to design $CaCO_3$-based materials with mechanical properties that more closely resemble those of natural counterparts with similar compositions.

Acknowledgements

H. Du would like to sincerely thank everyone in the biomineralization research community whose excellent work inspired, helped and motivated him throughout his PhD studies. We especially thank Prof. Jim De Yoreo and Dr. Alejandro Fernandez-Martinez for fruitful discussions. This work was financially supported by the Bio-Inspired Materials NCCR (SNSF).

Keywords: Bio-inspired materials•$CaCO_3$•Amorphous calcium carbonate•Water•Crystallization

[1] M. Eder, S. Amini, P. Fratzl, *Science* **2018**, *362*, 543–547.
[2] R. O. Ritchie, *Nat. Mater.* **2011**, *10*, 817–822.
[3] U. G. K. Wegst, H. Bai, E. Saiz, A. P. Tomsia, R. O. Ritchie, *Nat. Mater.* **2015**, *14*, 23–36.
[4] L. B. Gower, *Chem. Rev.* **2008**, *108*, 4551–4627.
[5] F. C. Meldrum, H. Cölfen, *Chem. Rev.* **2008**, *108*, 4332–4432.
[6] N. A. J. M. Sommerdijk, G. de With, *Chem. Rev.* **2008**, *108*, 4499–4550.
[7] E. Beniash, J. Aizenberg, L. Addadi, S. Weiner, *Proc. R. Soc. B Biol. Sci.* **1997**, *264*, 461–465.
[8] Y. Politi, *Science* **2004**, *306*, 1161–1164.
[9] L. Addadi, S. Raz, S. Weiner, *Adv. Mater.* **2003**, *15*, 959–970.
[10] Y. U. T. Gong, C. E. Killian, I. C. Olson, N. P. Appathurai, A. L. Amasino, M. C. Martin, L. J. Holt, F. H. Wilt, P. U. P. A. Gilbert, *Proc. Natl. Acad. Sci.* **2012**, *109*, 6088–6093.
[11] Y. Politi, R. A. Metzler, M. Abrecht, B. Gilbert, F. H. Wilt, I. Sagi, L. Addadi, S. Weiner, P. U. P. A. Gilbert, *Proc. Natl. Acad. Sci.* **2008**, *105*, 17362–17366.
[12] A. Sato, S. Nagasaka, K. Furihata, S. Nagata, I. Arai, K. Saruwatari, T. Kogure, S. Sakuda, H. Nagasawa, *Nat. Chem. Biol.* **2011**, *7*, 197–199.
[13] A. Akiva-Tal, S. Kababya, Y. S. Balazs, L. Glazer, A. Berman, A. Sagi, A. Schmidt, *Proc. Natl. Acad. Sci. U. S. A.* **2011**, *108*, 14763–14768.
[14] T. Mass, A. J. Giuffre, C.-Y. Sun, C. A. Stifler, M. J. Frazier, M. Neder, N. Tamura, C. V. Stan, M. A. Marcus, P. U. P. A. Gilbert, *Proc. Natl. Acad. Sci.* **2017**, *114*, E7670–E7678.
[15] R. T. DeVol, C.-Y. Sun, M. A. Marcus, S. N. Coppersmith, S. C. B. Myneni, P. U. P. A. Gilbert, *J. Am. Chem. Soc.* **2015**, *137*, 13325–13333.
[16] M. Rousseau, E. Lopez, P. Stempflé, M. Brendlé, L. Franke, A. Guette, R. Naslain, X. Bourrat, *Biomaterials* **2005**, *26*, 6254–6262.
[17] X. Li, W.-C. Chang, Y. J. Chao, R. Wang, M. Chang, *Nano Lett.* **2004**, *4*, 613–617.
[18] X. Li, Z.-H. Xu, R. Wang, *Nano Lett.* **2006**, *6*, 2301–2304.
[19] H. Du, U. Steiner, E. Amstad, *Chim. Int. J. Chem.* **2019**, *73*, 29–34.
[20] N. Koga, Y. Nakagoe, H. Tanaka, *Thermochim. Acta* **1998**, *318*, 239–244.
[21] P. Bots, L. G. Benning, J.-D. Rodriguez-Blanco, T. Roncal-Herrero, S. Shaw, *Cryst. Growth Des.* **2012**, *12*, 3806–3814.
[22] D. Pontoni, J. Bolze, N. Dingenouts, T. Narayanan, M. Ballauff, *J. Phys. Chem. B* **2003**, *107*, 5123–5125.
[23] M. H. Nielsen, S. Aloni, J. J. D. Yoreo, *Science* **2014**, *345*, 1158–1162.
[24] E. Loste, F. C. Meldrum, *Chem. Commun.* **2001**, 901–902.
[25] E. Loste, R. J. Park, J. Warren, F. C. Meldrum, *Adv. Funct. Mater.* **2004**, *14*, 1211–1220.
[26] Y.-Y. Kim, N. B. J. Hetherington, E. H. Noel, R. Kröger, J. M. Charnock, H. K. Christenson, F. C. Meldrum, *Angew. Chem. Int. Ed.* **2011**, *50*, 12572–12577.
[27] Y. Wen, L. Xiang, Y. Jin, *Mater. Lett.* **2003**, *57*, 2565–2571.
[28] K. Wang, Y. J. Wang, G. G. Chen, G. S. Luo, J. D. Wang, *Ind. Eng. Chem. Res.* **2007**, *46*, 6092–6098.
[29] C. Rodriguez-Navarro, K. Kudłacz, Ö. Cizer, E. Ruiz-Agudo, *CrystEngComm* **2015**, *17*, 58–72.
[30] H. Du, M. Steinacher, C. Borca, T. Huthwelker, A. Murello, F. Stellacci, E. Amstad, *J. Am. Chem. Soc.* **2018**, *140*, 14289–14299.
[31] J. Ihli, P. Bots, A. Kulak, L. G. Benning, F. C. Meldrum, *Adv. Funct. Mater.* **2013**, *23*, 1965–1973.
[32] P. J. M. Smeets, K. R. Cho, R. G. E. Kempen, N. A. J. M. Sommerdijk, J. J. De Yoreo, *Nat. Mater.* **2015**, *14*, 394–399.
[33] L. B. Gower, D. J. Odom, *J. Cryst. Growth* **2000**, 16.
[34] Y. Kitano, K. Park, D. W. Hood, *J. Geophys. Res. 1896-1977* **1962**, *67*, 4873–4874.
[35] S. E. Wolf, J. Leiterer, M. Kappl, F. Emmerling, W. Tremel, *J. Am. Chem. Soc.* **2008**, *130*, 12342–12347.
[36] E. M. Pouget, P. H. H. Bomans, J. A. C. M. Goos, P. M. Frederik, G. de With, N. A. J. M. Sommerdijk, *Science* **2009**, *323*, 1455–1458.
[37] J. Rudloff, H. Cölfen, *Langmuir* **2004**, *20*, 991–996.
[38] K. J. Davis, *Science* **2000**, *290*, 1134–1137.
[39] A. E. Stephenson, J. J. DeYoreo, L. Wu, K. J. Wu, J. Hoyer, P. M. Dove, *Science* **2008**, *322*, 724–727.
[40] Q. Hu, M. H. Nielsen, C. L. Freeman, L. M. Hamm, J. Tao, J. R. I. Lee, T. Y. J. Han, U. Becker, J. H. Harding, P. M. Dove, et al., *Faraday Discuss.* **2013**, *159*, 509–523.
[41] Y.-W. Wang, Y.-Y. Kim, C. J. Stephens, F. C. Meldrum, H. K. Christenson, *Cryst. Growth Des.* **2012**, *12*, 1212–1217.
[42] J. Rieger, J. Thieme, C. Schmidt, *Langmuir* **2000**, *16*, 8300–8305.
[43] J. D. Rodriguez-Blanco, S. Shaw, L. G. Benning, *Nanoscale* **2011**, *3*, 265–271.
[44] J. R. Clarkson, T. J. Price, C. J. Adams, *J. Chem. Soc. Faraday Trans.* **1992**, *88*, 243–249.
[45] D. Gebauer, M. Kellermeier, J. D. Gale, L. Bergström, H. Cölfen, *Chem. Soc. Rev.* **2014**, *43*, 2348–2371.
[46] P. J. M. Smeets, A. R. Finney, W. J. E. M. Habraken, F. Nudelman, H. Friedrich, J. Laven, J. J. De Yoreo, P. M. Rodger, N. A. J. M. Sommerdijk, *Proc. Natl. Acad. Sci.* **2017**, *114*, E7882–E7890.
[47] J. Rieger, M. Kellermeier, L. Nicoleau, *Angew. Chem. Int. Ed.* **2014**, *53*, 12380–12396.
[48] J. J. De Yoreo, P. U. P. A. Gilbert, N. A. J. M. Sommerdijk, R. L. Penn, S. Whitelam, D. Joester, H. Zhang, J. D. Rimer, A. Navrotsky, J. F. Banfield, et al., *Science* **2015**, *349*, aaa6760.
[49] D. Gebauer, A. Völkel, H. Cölfen, *Science* **2008**, *322*, 1819–1822.
[50] J. Rieger, T. Frechen, G. Cox, W. Heckmann, C. Schmidt, J. Thieme, *Faraday Discuss.* **2007**, *136*, 265–277.

[51] A. F. Wallace, L. O. Hedges, A. Fernandez-Martinez, P. Raiteri, J. D. Gale, G. A. Waychunas, S. Whitelam, J. F. Banfield, J. J. De Yoreo, *Science* **2013**, *341*, 885–889.
[52] A. S. A. Mohammed, A. Carino, A. Testino, M. R. Andalibi, A. Cervellino, *ArXiv181011696 Cond-Mat* **2018**.
[53] Y. Chao, O. Horner, P. Vallée, F. Meneau, O. Alos-Ramos, F. Hui, M. Turmine, H. Perrot, J. Lédion, *Langmuir* **2014**, *30*, 3303–3309.
[54] R. Demichelis, P. Raiteri, J. D. Gale, D. Quigley, D. Gebauer, *Nat. Commun.* **2011**, *2*, 590.
[55] M. Kellermeier, P. Raiteri, J. K. Berg, A. Kempter, J. D. Gale, D. Gebauer, *ChemPhysChem* **2016**, *17*, 3535–3541.
[56] K. Henzler, E. O. Fetisov, M. Galib, M. D. Baer, B. A. Legg, C. Borca, J. M. Xto, S. Pin, J. L. Fulton, G. K. Schenter, et al., *Sci. Adv.* **2018**, *4*, eaao6283.
[57] A. Carino, A. Testino, M. R. Andalibi, F. Pilger, P. Bowen, C. Ludwig, *Cryst. Growth Des.* **2017**, *17*, 2006–2015.
[58] M. Faatz, F. Gröhn, G. Wegner, *Adv. Mater.* **2004**, *16*, 996–1000.
[59] X. Cheng, P. L. Varona, M. J. Olszta, L. B. Gower, *J. Cryst. Growth* **2007**, *307*, 395–404.
[60] F. Sebastiani, S. L. P. Wolf, B. Born, T. Q. Luong, H. Cölfen, D. Gebauer, M. Havenith, *Angew. Chem. Int. Ed.* **2017**, *56*, 490–495.
[61] M. A. Bewernitz, D. Gebauer, J. Long, H. Cölfen, L. B. Gower, *Faraday Discuss.* **2012**, *159*, 291.
[62] S. E. Wolf, J. Leiterer, V. Pipich, R. Barrea, F. Emmerling, W. Tremel, *J. Am. Chem. Soc.* **2011**, *133*, 12642–12649.
[63] Y. Xu, K. C. H. Tijssen, P. H. H. Bomans, A. Akiva, H. Friedrich, A. P. M. Kentgens, N. A. J. M. Sommerdijk, *Nat. Commun.* **2018**, *9*, 2582.
[64] F. M. Michel, J. MacDonald, J. Feng, B. L. Phillips, L. Ehm, C. Tarabrella, J. B. Parise, R. J. Reeder, *Chem. Mater.* **2008**, *20*, 4720–4728.
[65] J. Ihli, W. C. Wong, E. H. Noel, Y.-Y. Kim, A. N. Kulak, H. K. Christenson, M. J. Duer, F. C. Meldrum, *Nat. Commun.* **2014**, *5*, 3169.
[66] J. Liu, J. Rieger, K. Huber, *Langmuir* **2008**, *24*, 8262–8271.
[67] D. Quigley, P. M. Rodger, *J. Chem. Phys.* **2008**, *128*, 221101.
[68] P. Raiteri, J. D. Gale, *J. Am. Chem. Soc.* **2010**, *132*, 17623–17634.
[69] Z. Zou, L. Bertinetti, Y. Politi, A. C. S. Jensen, S. Weiner, L. Addadi, P. Fratzl, W. J. E. M. Habraken, *Chem. Mater.* **2015**, *27*, 4237–4246.
[70] A. Navrotsky, *Proc. Natl. Acad. Sci.* **2004**, *101*, 12096–12101.
[71] G. A. Tribello, F. Bruneval, C. Liew, M. Parrinello, *J. Phys. Chem. B* **2009**, *113*, 11680–11687.
[72] J. Bolze, D. Pontoni, M. Ballauff, T. Narayanan, H. Cölfen, *J. Colloid Interface Sci.* **2004**, *277*, 84–94.
[73] J. Bolze, B. Peng, N. Dingenouts, P. Panine, T. Narayanan, M. Ballauff, *Langmuir* **2002**, *18*, 8364–8369.
[74] M. Albéric, L. Bertinetti, Z. Zou, P. Fratzl, W. Habraken, Y. Politi, *Adv. Sci.* **2018**, *5*, 1701000.
[75] A. V. Radha, T. Z. Forbes, C. E. Killian, P. U. P. A. Gilbert, A. Navrotsky, *Proc. Natl. Acad. Sci.* **2010**, *107*, 16438–16443.
[76] G. Wolf, C. Günther, *J. Therm. Anal. Calorim.* **2001**, *65*, 687–698.
[77] B. P. Pichon, P. H. H. Bomans, P. M. Frederik, N. A. J. M. Sommerdijk, *J. Am. Chem. Soc.* **2008**, *130*, 4034–4040.
[78] M. Saharay, A. O. Yazaydin, R. J. Kirkpatrick, *J. Phys. Chem. B* **2013**, *117*, 3328–3336.
[79] Y. G. Bushuev, A. R. Finney, P. M. Rodger, *Cryst. Growth Des.* **2015**, *15*, 5269–5279.
[80] E. M. Pouget, P. H. H. Bomans, A. Dey, P. M. Frederik, G. de With, N. A. J. M. Sommerdijk, *J. Am. Chem. Soc.* **2010**, *132*, 11560–11565.
[81] F. Nudelman, E. Sonmezler, P. H. H. Bomans, G. de With, N. A. J. M. Sommerdijk, *Nanoscale* **2010**, *2*, 2436.
[82] M. Farhadi Khouzani, D. M. Chevrier, P. Güttlein, K. Hauser, P. Zhang, N. Hedin, D. Gebauer, *CrystEngComm* **2015**, *17*, 4842–4849.
[83] C. C. Tester, R. E. Brock, C.-H. Wu, M. R. Krejci, S. Weigand, D. Joester, *CrystEngComm* **2011**, *13*, 3975–3978.
[84] D. Gebauer, P. N. Gunawidjaja, J. Y. P. Ko, Z. Bacsik, B. Aziz, L. Liu, Y. Hu, L. Bergström, C.-W. Tai, T.-K. Sham, et al., *Angew. Chem. Int. Ed.* **2010**, *49*, 8889–8891.
[85] M. Farhadi-Khouzani, D. M. Chevrier, P. Zhang, N. Hedin, D. Gebauer, *Angew. Chem. Int. Ed.* **2016**, *55*, 8117–8120.
[86] D. J. Tobler, J. D. Rodriguez Blanco, H. O. Sørensen, S. L. S. Stipp, K. Dideriksen, *Cryst. Growth Des.* **2016**, *16*, 4500–4508.
[87] J. H. E. Cartwright, A. G. Checa, J. D. Gale, D. Gebauer, C. I. Sainz-Díaz, *Angew. Chem. Int. Ed.* **2012**, *51*, 11960–11970.
[88] A. L. Goodwin, F. M. Michel, B. L. Phillips, D. A. Keen, M. T. Dove, R. J. Reeder, *Chem. Mater.* **2010**, *22*, 3197–3205.
[89] C. J. Stephens, S. F. Ladden, F. C. Meldrum, H. K. Christenson, *Adv. Funct. Mater.* **2010**, *20*, 2108–2115.
[90] S. Weiner, Y. Levi-Kalisman, S. Raz, L. Addadi, *Connect. Tissue Res.* **2003**, *44*, 214–218.
[91] S. Gunasekaran, G. Anbalagan, S. Pandi, *J. Raman Spectrosc.* **2006**, *37*, 892–899.
[92] H. Nebel, M. Neumann, C. Mayer, M. Epple, *Inorg. Chem.* **2008**, *47*, 7874–7879.
[93] S. Sun, D. M. Chevrier, P. Zhang, D. Gebauer, H. Cölfen, *Angew. Chem. Int. Ed.* **2016**, *55*, 12206–12209.
[94] I. Ben Shir, S. Kababya, I. Katz, B. Pokroy, A. Schmidt, *Chem. Mater.* **2013**, *25*, 4595–4602.
[95] S. Sen, D. C. Kaseman, B. Colas, D. E. Jacob, S. M. Clark, *Phys. Chem. Chem. Phys.* **2016**, *18*, 20330–20337.
[96] A. Becker, U. Bismayer, M. Epple, H. Fabritius, B. Hasse, J. Shi, A. Ziegler, *Dalton Trans.* **2003**, *0*, 551–555.
[97] Y. Levi-Kalisman, S. Raz, S. Weiner, L. Addadi, I. Sagi, *Adv. Funct. Mater.* **2002**, *12*, 43.
[98] R. S. K. Lam, J. M. Charnock, A. Lennie, F. C. Meldrum, *CrystEngComm* **2007**, *9*, 1226.
[99] C. Günther, A. Becker, G. Wolf, M. Epple, *Z. Für Anorg. Allg. Chem.* **2005**, *631*, 2830–2835.
[100] M. P. Schmidt, A. J. Ilott, B. L. Phillips, R. J. Reeder, *Cryst. Growth Des.* **2014**, *14*, 938–951.
[101] J. W. Singer, A. Ö. Yazaydin, R. J. Kirkpatrick, G. M. Bowers, *Chem. Mater.* **2012**, *24*, 1828–1836.
[102] R. Innocenti Malini, Y. G. Bushuev, S. A. Hall, C. L. Freeman, P. M. Rodger, J. H. Harding, *CrystEngComm* **2016**, *18*, 92–101.
[103] G. Cobourne, G. Mountjoy, J. D. Rodriguez-Blanco, L. G. Benning, A. C. Hannon, J. R. Plaisier, *J. Non-Cryst. Solids* **2014**, *401*, 154–158.
[104] A. C. S. Jensen, S. Imberti, S. F. Parker, E. Schneck, Y. Politi, P. Fratzl, L. Bertinetti, W. J. E. M. Habraken, *J. Phys. Chem. C* **2018**, *122*, 3591–3598.
[105] A. Fernandez-Martinez, B. Kalkan, S. M. Clark, G. A. Waychunas, *Angew. Chem. Int. Ed.* **2013**, *52*, 8354–8357.
[106] M. Saharay, R. James Kirkpatrick, *Chem. Phys. Lett.* **2014**, *591*, 287–291.
[107] H. Tomono, H. Nada, F. Zhu, T. Sakamoto, T. Nishimura, T. Kato, *J. Phys. Chem. B* **2013**, *117*, 14849–14856.
[108] J. Ihli, A. N. Kulak, F. C. Meldrum, *Chem. Commun.* **2013**, *49*, 3134.
[109] M. Saharay, R. J. Kirkpatrick, *Phys. Chem. Chem. Phys.* **2017**, *19*, 29594–29600.
[110] N. Koga, Y. Yamane, *J. Therm. Anal. Calorim.* **2008**, *94*, 379–387.
[111] X. Xu, J. T. Han, D. H. Kim, K. Cho, *J. Phys. Chem. B* **2006**, *110*, 2764–2770.
[112] F. Konrad, F. Gallien, D. E. Gerard, M. Dietzel, *Cryst. Growth Des.* **2016**, *16*, 6310–6317.
[113] A. Gal, W. Habraken, D. Gur, P. Fratzl, S. Weiner, L. Addadi, *Angew. Chem. Int. Ed.* **2013**, *52*, 4867–4870.
[114] A. Gal, K. Kahil, N. Vidavsky, R. T. DeVol, P. U. P. A. Gilbert, P. Fratzl, S. Weiner, L. Addadi, *Adv. Funct. Mater.* **2014**, *24*, 5420–5426.
[115] T. Yoshino, K. Maruyama, H. Kagi, M. Nara, J. C. Kim, *Cryst. Growth Des.* **2012**, *12*, 3357–3361.
[116] K. Maruyama, H. Kagi, T. Inoue, H. Ohfuji, T. Yoshino, *Chem. Lett.* **2015**, *44*, 434–436.
[117] Y. G. Bushuev, A. R. Finney, P. M. Rodger, *Cryst. Growth Des.* **2015**, *15*, 5269–5279.

[118] A. J. Giuffre, A. C. Gagnon, J. J. De Yoreo, P. M. Dove, *Geochim. Cosmochim. Acta* **2015**, *165*, 407–417.
[119] A. S. Schenk, E. J. Albarracin, Y.-Y. Kim, J. Ihli, F. C. Meldrum, *Chem Commun* **2014**, *50*, 4729–4732.
[120] M. Zeng, Y.-Y. Kim, C. Anduix-Canto, C. Frontera, D. Laundy, N. Kapur, H. K. Christenson, F. C. Meldrum, *Proc. Natl. Acad. Sci.* **2018**, *115*, 7670–7675.
[121] A. A. Noyes, W. R. Whitney, *J. Am. Chem. Soc.* **1897**, *19*, 930–934.
[122] J. D. Rodriguez-Blanco, S. Shaw, P. Bots, T. Roncal-Herrero, L. G. Benning, *J. Alloys Compd.* **2012**, *536*, S477–S479.
[123] X. R. Xu, A. H. Cai, R. Liu, H. H. Pan, R. K. Tang, K. Cho, *J. Cryst. Growth* **2008**, *310*, 3779–3787.
[124] S.-F. Chen, H. Cölfen, M. Antonietti, S.-H. Yu, *Chem. Commun.* **2013**, *49*, 9564.
[125] M. L. Dundon, E. Mack, *J. Am. Chem. Soc.* **1923**, *45*, 2479–2485.
[126] Y. Kojima, A. Kawanobe, T. Yasue, Y. Arai, *J. Ceram. Soc. Jpn.* **1993**, *101*, 1145–1152.
[127] C. C. Tester, C.-H. Wu, S. Weigand, D. Joester, *Faraday Discuss.* **2013**, *159*, 345–356.
[128] C. C. Tester, M. L. Whittaker, D. Joester, *Chem. Commun.* **2014**, *50*, 5619–5622.
[129] C. J. Stephens, Y.-Y. Kim, S. D. Evans, F. C. Meldrum, H. K. Christenson, *J. Am. Chem. Soc.* **2011**, *133*, 5210–5213.
[130] M. L. Whittaker, P. M. Dove, D. Joester, *MRS Bull.* **2016**, *41*, 388–392.
[131] D. Gebauer, H. Cölfen, A. Verch, M. Antonietti, *Adv. Mater.* **2009**, *21*, 435–439.
[132] A. Verch, D. Gebauer, M. Antonietti, H. Cölfen, *Phys. Chem. Chem. Phys.* **2011**, *13*, 16811.
[133] D. Gebauer, Denis, *Minerals* **2018**, *8*, 179.
[134] J. Aizenberg, L. Addadi, S. Weiner, G. Lambert, *Adv. Mater.* **1996**, *8*, 222–226.
[135] J. Ihli, Y.-Y. Kim, E. H. Noel, F. C. Meldrum, *Adv. Funct. Mater.* **2013**, *23*, 1575–1585.
[136] F. Nudelman, N. A. J. M. Sommerdijk, *Angew. Chem. Int. Ed.* **2012**, *51*, 6582–6596.
[137] A.-W. Xu, Y. Ma, H. Cölfen, *J. Mater. Chem.* **2007**, *17*, 415–449.
[138] Y.-Y. Kim, J. D. Carloni, B. Demarchi, D. Sparks, D. G. Reid, M. E. Kunitake, C. C. Tang, M. J. Duer, C. L. Freeman, B. Pokroy, et al., *Nat. Mater.* **2016**, *15*, 903–910.
[139] L.-B. Mao, H.-L. Gao, H.-B. Yao, L. Liu, H. Colfen, G. Liu, S.-M. Chen, S.-K. Li, Y.-X. Yan, Y.-Y. Liu, et al., *Science* **2016**, *354*, 107–110.
[140] J. Aizenberg, D. A. Muller, J. L. Grazul, D. R. Hamann, *Science* **2003**, *299*, 1205–1208.
[141] B. Cantaert, D. Kuo, S. Matsumura, T. Nishimura, T. Sakamoto, T. Kato, *ChemPlusChem* **2017**, *82*, 107–120.
[142] T. Sakamoto, A. Oichi, T. Nishimura, A. Sugawara, T. Kato, *Polym. J.* **2009**, *41*, 522–523.
[143] A. Finnemore, P. Cunha, T. Shean, S. Vignolini, S. Guldin, M. Oyen, U. Steiner, *Nat. Commun.* **2012**, *3*, 966.
[144] J. Xiao, S. Yang, *Nanoscale* **2012**, *4*, 54–65.
[145] E. Loste, R. M. Wilson, R. Seshadri, F. C. Meldrum, *J. Cryst. Growth* **2003**, *254*, 206–218.
[146] B. Purgstaller, V. Mavromatis, A. Immenhauser, M. Dietzel, *Geochim. Cosmochim. Acta* **2016**, *174*, 180–195.
[147] C. R. Blue, A. Giuffre, S. Mergelsberg, N. Han, J. J. De Yoreo, P. M. Dove, *Geochim. Cosmochim. Acta* **2017**, *196*, 179–196.
[148] H. Yang, S. Chai, Y. Zhang, Y. Ma, *CrystEngComm* **2015**, *18*, 157–163.
[149] Y.-C. Huang, M. B. Gindele, J. Knaus, A. Rao, D. Gebauer, *CrystEngComm* **2018**, *20*, 4395–4405.
[150] Z. Zou, W. J. E. M. Habraken, G. Matveeva, A. C. S. Jensen, L. Bertinetti, M. A. Hood, C. Sun, P. U. P. A. Gilbert, I. Polishchuk, B. Pokroy, et al., *Science* **2019**, *363*, 396–400.
[151] A. V. Radha, A. Fernandez-Martinez, Y. Hu, Y.-S. Jun, G. A. Waychunas, A. Navrotsky, *Geochim. Cosmochim. Acta* **2012**, *90*, 83–95.
[152] R. M. Noyes, *J. Am. Chem. Soc.* **1962**, *84*, 513–522.
[153] A. Mucci, J. W. Morse, *Geochim. Cosmochim. Acta* **1983**, *47*, 217–233.
[154] Z. Zhang, Y. Xie, X. Xu, H. Pan, R. Tang, *J. Cryst. Growth* **2012**, *343*, 62–67.
[155] A. Koishi, A. Fernandez-Martinez, B. Ruta, M. Jimenez-Ruiz, R. Poloni, D. di Tommaso, F. Zontone, G. A. Waychunas, G. Montes-Hernandez, *J. Phys. Chem. C* **2018**, *122*, 16983–16991.
[156] E. Dimasi, S. Y. Kwak, F. F. Amos, M. J. Olszta, D. Lush, L. B. Gower, *Phys. Rev. Lett.* **2006**, *97*, 45503.
[157] Z. Zou, I. Polishchuk, L. Bertinetti, B. Pokroy, Y. Politi, P. Fratzl, W. J. E. M. Habraken, *J. Mater. Chem. B* **2018**, *6*, 449–457.
[158] J. Jiang, M.-R. Gao, Y.-H. Qiu, S.-H. Yu, *Nanoscale* **2010**, *2*, 2358–2361.
[159] S.-Y. Yang, H.-H. Chang, C.-J. Lin, S.-J. Huang, J. C. C. Chan, *Chem. Commun.* **2016**, *52*, 11527–11530.
[160] D. D. Tommaso, N. H. de Leeuw, *Phys. Chem. Chem. Phys.* **2010**, *12*, 894–901.
[161] Y. Politi, D. R. Batchelor, P. Zaslansky, B. F. Chmelka, J. C. Weaver, I. Sagi, S. Weiner, L. Addadi, *Chem. Mater.* **2010**, *22*, 161–166.
[162] J. D. Rodriguez-Blanco, S. Shaw, P. Bots, T. Roncal-Herrero, L. G. Benning, *Geochim. Cosmochim. Acta* **2014**, *127*, 204–220.
[163] P.-T. Yu, C. Tsao, C.-C. Wang, C.-Y. Chang, C.-H. Wang, J. C. C. Chan, *Angew. Chem. Int. Ed.* **2017**, *56*, 16202–16206.
[164] M. E. Kunitake, S. P. Baker, L. A. Estroff, *MRS Commun.* **2012**, *2*, 113–116.
[165] C.-J. Lin, S.-Y. Yang, S.-J. Huang, J. C. C. Chan, *J. Phys. Chem. C* **2015**, *119*, 7225–7233.
[166] D. J. Tobler, J. D. Rodriguez-Blanco, K. Dideriksen, N. Bovet, K. K. Sand, S. L. S. Stipp, *Adv. Funct. Mater.* **2015**, *25*, 3081–3090.
[167] D. J. Tobler, J. D. R. Blanco, K. Dideriksen, K. K. Sand, N. Bovet, L. G. Benning, S. L. S. Stipp, *Procedia Earth Planet. Sci.* **2014**, *10*, 143–148.
[168] S. Kababya, A. Gal, K. Kahil, S. Weiner, L. Addadi, A. Schmidt, *J. Am. Chem. Soc.* **2015**, *137*, 990–998.
[169] A. W. Xu, Q. Yu, W. F. Dong, M. Antonietti, H. Cölfen, *Adv. Mater.* **2005**, *17*, 2217–2221.
[170] S. Bentov, S. Weil, L. Glazer, A. Sagi, A. Berman, *J. Struct. Biol.* **2010**, *171*, 207–215.
[171] L. . Plant, W. . House, *Colloids Surf. Physicochem. Eng. Asp.* **2002**, *203*, 143–153.
[172] H. J. Meyer, *J. Cryst. Growth* **1984**, *66*, 639–646.
[173] G. Montanari, L. Z. Lakshtanov, D. J. Tobler, K. Dideriksen, K. N. Dalby, N. Bovet, S. L. S. Stipp, *Cryst. Growth Des.* **2016**, *16*, 4813–4821.
[174] C. A. Orme, A. Noy, A. Wierzbicki, M. T. McBride, M. Grantham, H. H. Teng, P. M. Dove, J. J. DeYoreo, *Nature* **2001**, *411*, 775–779.
[175] D. C. Green, J. Ihli, Y.-Y. Kim, S. Y. Chong, P. A. Lee, C. J. Empson, F. C. Meldrum, *Cryst. Growth Des.* **2016**, *16*, 5174–5183.
[176] G. Montanari, J. D. Rodriguez-Blanco, N. Bovet, S. L. S. Stipp, D. J. Tobler, *Cryst. Growth Des.* **2017**, *17*, 5269–5275.
[177] W. Jiang, M. S. Pacella, D. Athanasiadou, V. Nelea, H. Vali, R. M. Hazen, J. J. Gray, M. D. McKee, *Nat. Commun.* **2017**, *8*, 15066.
[178] B. Cantaert, Y.-Y. Kim, H. Ludwig, F. Nudelman, N. A. J. M. Sommerdijk, F. C. Meldrum, *Adv. Funct. Mater.* **2012**, *22*, 907–915.
[179] V. Dmitrovic, G. J. M. Habraken, M. M. R. M. Hendrix, W. J. E. M. Habraken, A. Heise, G. De With, N. A. J. M. Sommerdijk, *Polymers* **2012**, *4*, 1195–1210.
[180] A. Rao, P. Vásquez-Quitral, M. S. Fernández, J. K. Berg, M. Sánchez, M. Drechsler, A. Neira-Carrillo, J. L. Arias, D. Gebauer, H. Cölfen, *Cryst. Growth Des.* **2016**, *16*, 1349–1359.
[181] E. Weber, I. M. Weiss, H. Cölfen, M. Kellermeier, *CrystEngComm* **2016**, *18*, 8439–8444.
[182] Z. Zou, L. Bertinetti, Y. Politi, P. Fratzl, W. J. E. M. Habraken, *Small* **2017**, *13*, 1603100.
[183] B. Guillemet, M. Faatz, F. Gröhn, G. Wegner, Y. Gnanou, *Langmuir* **2006**, *22*, 1875–1879.
[184] M. Kellermeier, E. Melero-García, F. Glaab, R. Klein, M. Drechsler, R. Rachel, J. M. García-Ruiz, W. Kunz, *J. Am. Chem. Soc.* **2010**, *132*, 17859–17866.

[185] S. Elhadj, E. A. Salter, A. Wierzbicki, J. J. De Yoreo, N. Han, P. M. Dove, *Cryst. Growth Des.* **2006**, *6*, 197–201.
[186] T. Wang, M. Antonietti, H. Cölfen, *Chem. – Eur. J.* **2006**, *12*, 5722–5730.
[187] T. Wang, H. Cölfen, M. Antonietti, *J. Am. Chem. Soc.* **2005**, *127*, 3246–3247.
[188] S. L. P. Wolf, K. Jähme, D. Gebauer, *CrystEngComm* **2015**, *17*, 6857–6862.
[189] D. Wang, A. F. Wallace, J. J. De Yoreo, P. M. Dove, *Proc. Natl. Acad. Sci.* **2009**, *106*, 21511–21516.
[190] Y. Ma, S. R. Cohen, L. Addadi, S. Weiner, *Adv. Mater.* **2008**, *20*, 1555–1559.

Entry for the Table of Contents

REVIEW

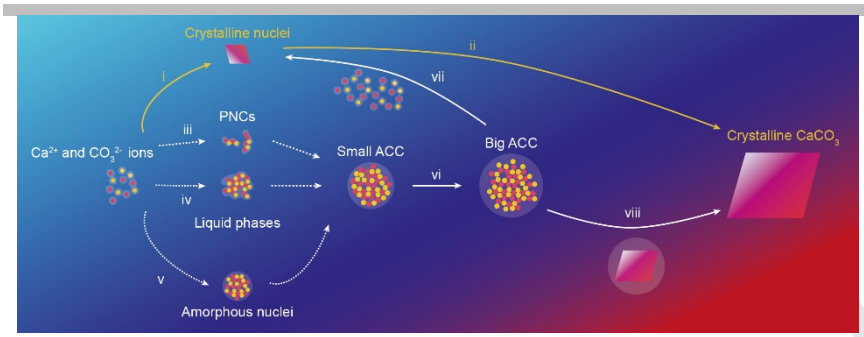

Inspired by the fascinating properties of biomineral-based materials produced by nature, a lot of work has been dedicated to studying the formation of biominerals. In this review, we summarize the current understanding on the formation of $CaCO_3$, one of the most abundant biominerals. We put special emphasis on the roles of water in mediating the formation of $CaCO_3$, an often overlooked aspect that is of high relevance.

*Huachuan Du, Esther Amstad**

Page No. – Page No.

Water: How does it influence the $CaCO_3$ formation?